

Thermal Slip Length at a Liquid/Solid Interface: Power Law Relations From Spatial and Frequency Attributes of the Contact Layer

Hiroki Kaifu and Sandra M. Troian*

California Institute of Technology, T. J. Watson Sr. Laboratories of Applied Physics, MC 128-95, Pasadena, CA 91125

(Dated: October 16, 2024)

Specialty integrated chips for power intensive tasks like artificial intelligence generate so much heat that data centers are switching to liquid cooling to prevent malfunction. A critical factor hindering optimization of the thermal flux across the liquid/solid (L/S) interface is the lack of any predictive model for the thermal slip length at non-cryogenic temperatures. An extensive study using non-equilibrium molecular dynamics simulations reveals distinct power law relations governing this length scale which incorporate the influence of local temperature, in-plane translational order and vibrational frequency of the liquid contact layer and adjoining solid layer. Similar relations are expected to hold for other L/S systems modeled by the Lennard-Jones potential given the principle of corresponding states.

I. INTRODUCTION

Powerful chips specially designed for extensive data mining required by artificial intelligence and cryptocurrency exchange generate such tremendous heat in such small volumes that the industry has had to pivot from air to liquid cooling to prevent nucleation of hot spots and deleterious thermal runaway [1–3]. Although challenging to implement because of the ultra compact architecture of today’s integrated circuits, liquid cooling has also shown benefit in increasing clock speeds and overall performance of conventional CMOS and superconducting processors, solid-state quantum devices [4] and the like. Despite the use of specialty liquid coolants and optimized flow patterns, there remains the ultimate challenge of minimizing to the degree possible the intrinsic thermal barrier posed by the liquid/solid (L/S) interface. Unfortunately, there exists no model for computing or estimating the L/S thermal slip length at non-cryogenic temperatures. This stands in contrast to L/S systems in low temperature physics for which the acoustic mismatch model [5] and diffusive mismatch model [6] yield useful bounds on the thermal Kapitza resistance [7] or Kapitza length.

This situation poses a fundamental problem since the boundary condition for solving the energy equation for thermal transport is unknown. While not so problematic for macroscale systems where the effects of the interfacial region are negligible, thermal barrier effects at the interface can be appreciable in nanoscale systems. A similar problem arises in fluid dynamics where the velocity boundary condition at an L/S interface for solving Cauchy’s equation of motion or the Navier-Stokes equation was also not known and so phenomenological models were introduced. Recent studies based on non-equilibrium molecular dynamics (NEMD) simulations unveiled key scaling relations used instead [8–12].

For a thermal flux along the \hat{z} axis crossing the L/S interface, this thermal barrier across the L/S boundary is quantified by the thermal slip length

$$L_T = \frac{\Delta T}{|dT/dz|_{liq}}, \quad (1)$$

where ΔT is the temperature jump at the interface and $|dT/dz|_{liq}$ is the magnitude of the thermal gradient within the liquid interior. For an isotropic liquid and solid with thermal conductivity $k(T)$ governed by Fourier’s law, at steady state conditions the thermal flux $J_z = k(T)|dT/dz|$ must be everywhere constant within the bulk material as well as in the interfacial region. The L/S interface can be regarded as a frequency filter which meters those collective vibrations allowed to cross the barrier.

NEMD studies have revealed various associations linking the thermal slip length to parameters such as the wettability of the L/S interface [13–18], liquid pressure [19, 20], solid temperature [21, 22], surface roughness [18], solid symmetry [23–25], liquid thickness [26], density depletion layer [27–29] and more. However, no predictive relations for quantifying L_T have been proposed. In this work, we focus on the spatial coherence and vibrational spectrum of the liquid contact layer [25] under the influence of a crystal surface potential. The results, which cover a wide parameter range, reveal distinct power law relations governing the magnitude of the thermal slip length. These relations reveal how the local temperature, peak value of the in-plane structure factor and peak vibrational frequency of the contact layer regulate the thermal flux across the L/S boundary.

II. COMPUTATIONAL DETAILS

We briefly outline essential features of the simulations and analysis; complete details and all measured values can be found in the Appendix. The geometry in Fig. 7 (a)-(b) describes a simple liquid flanked by the [001] facet of two face-centered cubic (FCC) crystals, which in turn are in direct contact with two external FCC layers

* Corresponding author:
stroian@caltech.edu; www.troian.caltech.edu

acting as Langevin thermostats with set point temperatures (T_{source} , T_{sink}). Particles in the liquid (L) and solid (S) layers were of equal mass and made to interact via a truncated and shifted Lennard-Jones (LJ) potential with energy and length scale ε_{ij} and σ_{ij} , respectively. Subscripts i, j refer to L/L , S/S and L/S interactions. In this study, the layer thicknesses and input parameters $\sigma_{SS} = 1.0$, $\sigma_{LL} = 1.0$, $\varepsilon_{LL} = 1.0$ and $\varepsilon_{SS} = 10$ remained fixed for all runs. The parameters that were varied included $(T_{\text{source}}, T_{\text{sink}}) = (1.8, 0.8), (1.6, 1.0)$ or $(1.4, 1.2)$, $\sigma_{LS} = 0.8, 1.0$ or 1.2 and $\varepsilon_{LS} = 0.1, 0.2, \dots, 0.9, 1.0$. The selections $(T_{\text{source}}, T_{\text{sink}})$ ensured that the average temperature of the liquid interior remained at $T = 1.3$, ensuring a dense fluid far from any critical or triple point [30, 31]. Measurements were extracted from the hotter

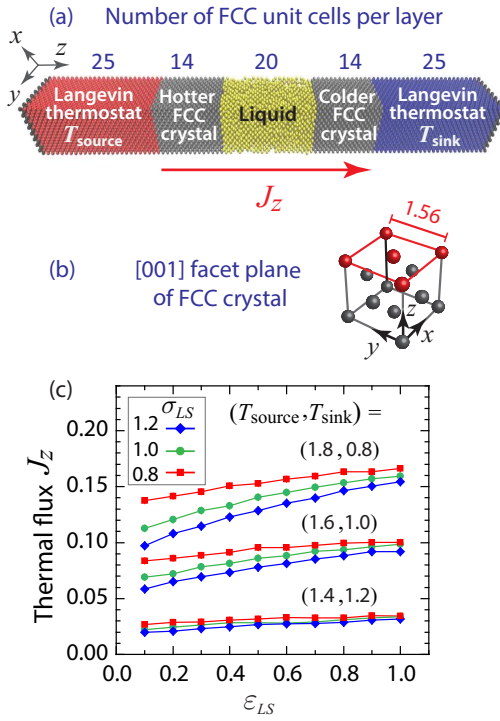


FIG. 1. (a) Computational geometry with T_{source} and T_{sink} fixed by Langevin thermostats. (b) [001] facet plane of FCC unit cell with edge length 1.56. (c) Dependence of thermal flux J_z on specified parameter values.

and colder side of the liquid layer to ascertain the influence of contact layer temperature T_c . Measured quantities (scaled by standard LJ reduced units), included the thermal flux J_z , interface temperature jump ΔT , thermal slip length L_T , contact layer temperature T_c , contact layer peak density ρ_c , interface density depletion layer thickness δ_{LS} , contact layer in-plane structure factor $S_c^{\parallel}(\vec{k})$ and per particle density of states $\mathcal{D}(\nu)$ of particles in the contact and first solid layer. Measured speeds in these layers confirmed Maxwell-Boltzmann statistics so that layer temperatures could be extracted from the equipartition relation.

Long range translational order in the contact (c) layer

induced by the crystal surface potential was evaluated from the in-plane (\parallel) static structure factor [32]

$$S_c^{\parallel}(\vec{k}) = \left\langle \frac{1}{N_c^2} \sum_{p=1}^{N_c} \sum_{q=1}^{N_c} \exp[i\vec{k} \cdot (\vec{r}_p - \vec{r}_q)] \right\rangle, \quad (2)$$

normalized by $S_c^{\parallel}(\vec{k} = 0)$ such that $0 \leq S_c^{\parallel}(\vec{k}) \leq 1$. Here, $\vec{r} = (x, y)$, $\vec{k} = (k_x, k_y)$, N_c is the number of particles in the contact layer and the angular brackets denote ensemble averaging. In this study, the maxima of Eq. (A.12) denoted $S_{\max} = S_{\max}(\vec{k}_o)$ always coincided with the set of smallest reciprocal lattice vectors \vec{k}_o of the [001] facet plane. The per particle density of states $\mathcal{D}(\nu)$ for the contact and first solid layer reflecting the normal mode vibrational spectrum was computed from the relation [33, 34]

$$\mathcal{D}(\nu) = \left\langle \frac{4}{N_L T_L} \int_0^{t_f} \sum_{j=1}^{N_L} \vec{v}_j(t_o + t) \cdot \vec{v}_j(t_o) \cos(2\pi i \nu t) dt \right\rangle_B, \quad (3)$$

where bracket superscripts denote ensemble averaging over t_o followed by block (B) averaging, $\vec{v} = (v_x, v_y, v_z)$, T_L is the layer temperature and $N_L = N_L(t_o, t_f)$ is the number of particles in the layer at t_o which remained there through t_f , never having exited. To ensure good statistics, the constraint imposed on the contact layer was $N_L = N_L(t_o, t_f) \geq 10$.

III. RESULTS

Shown in Fig. 7(c) is the increase in thermal flux J_z achieved by increasing $T_{\text{source}} - T_{\text{sink}}$, increasing ε_{LS} or decreasing σ_{LS} . For fixed values $(T_{\text{source}}, T_{\text{sink}})$ and ε_{LS} , the highest thermal flux is always achieved with the smallest value σ_{LS} ; however, the influence of σ_{LS} weakens considerably as ε_{LS} increases. The temperature jump ΔT at the hotter (H) and colder (C) interface plotted in Fig. 2 indicate several trends. A smaller thermal barrier, as quantified by smaller values ΔT , is generated with smaller values $T_{\text{source}} - T_{\text{sink}}$, larger ε_{LS} or smaller σ_{LS} . For fixed values $(T_{\text{source}}, T_{\text{sink}})$ and ε_{LS} , ΔT is always smallest for $\sigma_{LS} = 0.8$. While these trends are somewhat anticipated, others are not. For example, higher collision frequency between particles in the contact and first solid layer at higher temperatures might lead one to conclude that ΔT is always smaller at the hotter interface for fixed values $(T_{\text{source}}, T_{\text{sink}})$, ε_{LS} and σ_{LS} . However, this is not the case for certain parameter values as evident in Fig. 2(a) and (b) (and from the entries in Tables VI - VIII of the Appendix.) Similar intuition about thermally activated collisions has led to a prevailing misconception that a higher peak contact density ρ_c always correlates with a reduction in ΔT [35, 36]. However, simulations with larger parameter sets [25] have demonstrated this is not the case, as evident in this study too (Tables VI-VIII in the Supplemental Material). The point to emphasize is that correlations for L_T only involving primary input variables like $(T_{\text{source}}, T_{\text{sink}})$, ε_{LS}

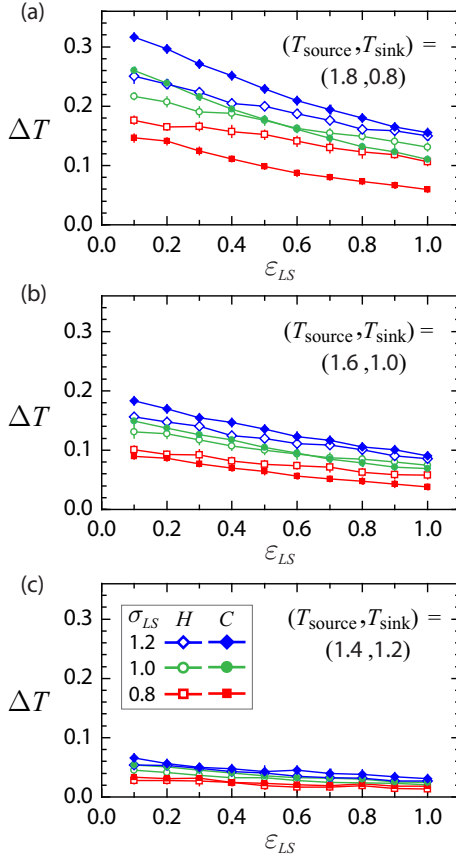


FIG. 2. Influence of $(T_{\text{source}}, T_{\text{sink}})$, ε_{LS} and σ_{LS} on ΔT for the hotter (H) and colder (C) L/S interface.

and σ_{LS} or simple metrics like ρ_c cannot capture those coherent structural and dynamic features of the interface responsible for enabling phonon vibrations across the L/S boundary. NEMD studies of velocity slip at an L/S interface in relative motion at isothermal conditions have drawn strong inverse correlation between the velocity slip length and the structure factor of the contact layer [9–12, 37]. Plotted in Fig. 3(a) - (c) are results of this study demonstrating how stronger L/S coupling - enforced by larger ε_{LS} , smaller σ_{LS} and/or lower T_c - causes larger values S_{max} . Closer inspection reveals that of the 180 systems examined, there are six cases with $S_{\text{max}} > 0.8$ which manifest saturation of S_{max} as $\varepsilon_{\text{LS}} \rightarrow 1.0$. This behavior, which suggests quasi-solidification or an epitaxially locked contact layer strongly bound to the crystal surface potential, contrasts sharply with the monotonic increase observed in all other cases. In Fig. 3(a)-(c), there is also evidence in the colder contact layers of a sharp transition from solid-like to liquid-like behavior for $\sigma_{\text{LS}} = 0.8$ as ε_{LS} increases from 0.1 to 0.2. Shown in Fig. 3(d)-(f) is the systematic reduction in L_T with increasing S_{max} . The similarity of these curves and dependence on $T_{\text{source}} - T_{\text{sink}}$ highlights the influence of T_c . Exclusive of the six data points where $S_{\text{max}} > 0.8$ noted above, the data covering 174 systems in Fig. 4 are well captured by

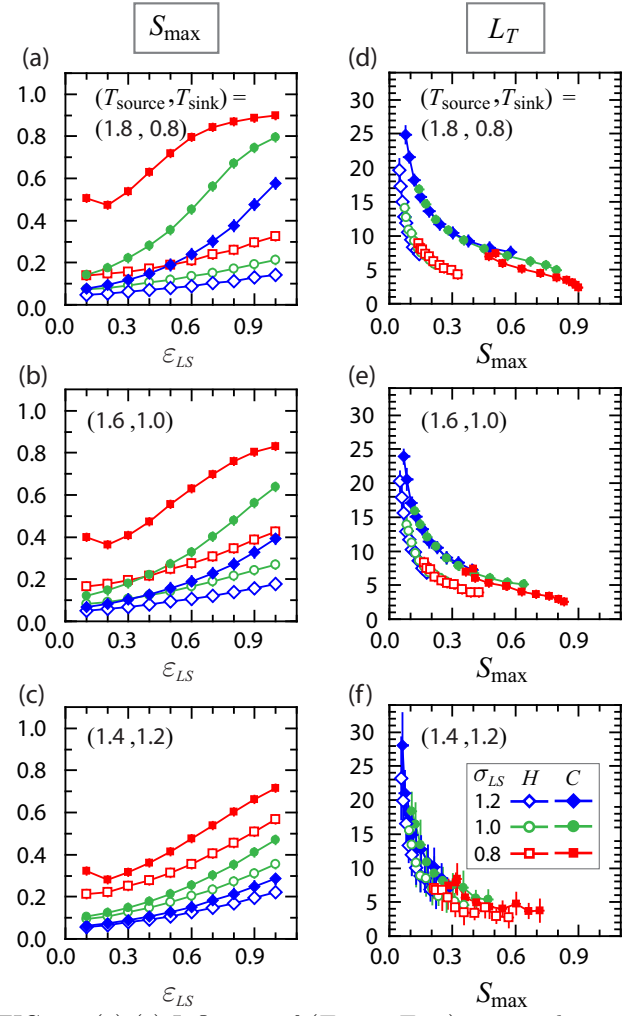


FIG. 3. (a)-(c) Influence of $(T_{\text{source}}, T_{\text{sink}})$, ε_{LS} and σ_{LS} on S_{max} for the hotter (H) and colder (C) contact layer. (d)-(f) Reduction in L_T with increasing S_{max} . Legend in (f) for (a)-(e) also.

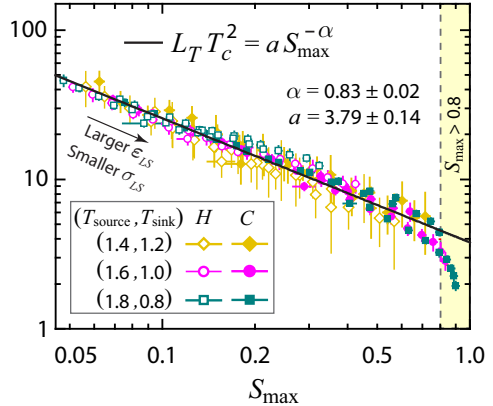


FIG. 4. Rescaled data with best fit to Eq. (4) (solid line) for 174 systems exclusive of six points with $S_{\text{max}} > 0.8$.

the equation

$$L_T T_c^2 = a S_{\text{max}}^{-\alpha} . \quad (4)$$

A nonlinear best fit to Eq. (4) using orthogonal distance regression to account for the error bars in measurements of L_T , T_c and S_{\max} yielded an exponent $\alpha = 0.83 \pm 0.02$ and coefficient $a = 3.79 \pm 0.14$ ($\pm 95\%$ confidence levels). Reducing the exponent of T_c from 2 to 1.5 resulted in $\alpha = 0.74 \pm 0.02$ and $a \simeq 3.94 \pm 0.16$, but the residual sum of squares increased by 20%. Regression with three variables generated a slight decrease in α from 0.83 ± 0.02 to 0.80 ± 0.03 and the T_c exponent from 2 to 1.83 ± 0.10 . These fitting procedures suggest the relation $L_T \sim T_c^{-2} S_{\max}^{4/5}$ although studies on different systems are needed to pin down the exponents. Nonetheless, the collapse of the data confirms how strongly the long range translational order in the contact layer, as modulated by the layer temperature, controls the magnitude of the thermal slip length.

Given this finding, we examined the combined influence on L_T of T_c , σ_{LS} and the ratio of peak vibrational frequencies of the contact layer ν_L and first solid layer ν_S . Typical distributions $\mathcal{D}(\nu)$ of these layers are plotted in Fig. 5(a). All things equal, as ε_{LS} increases from 0.1 to 1.0, the value [34] $\mathcal{D}(\nu = 0)$, which equals $12D/T_c$ [34] where D is the diffusion coefficient, diminishes considerably, reflecting the reduced mobility of particles within a completely wetting layer. This also produces a noticeable shift in ν_L and to lesser extent ν_S to higher frequencies. The results in Fig. 5(b)-(d) confirm that stronger L/S coupling - either enforced by larger ε_{LS} , smaller σ_{LS} and/or lower T_c - generates smaller ratios ν_S/ν_L indicative of better frequency matching. The six data points in Fig. 5(b)-(d) with $\varepsilon_{LS} = 0.1$ and $\sigma_{LS} = 0.8$ are somewhat surprising in that $\nu_S/\nu_L \approx 2$ despite these contact layers are highly non-wetting. This ratio ν_S/ν_L must also influence the thermal slip length. Shown in Fig. 6 is a collapse of the data covering 174 systems where the curve represents the equation

$$L_T T_c^{3/2} / \sigma_{LS}^2 = b \left(\nu_S / \nu_L \right)^\beta. \quad (5)$$

A nonlinear best fit to Eq. (5) using orthogonal distance regression to account for the error bars errors in L_T , T_c and ν_S/ν_L yielded the exponent $\beta = 2.93 \pm 0.11$ and coefficient $b = 0.35 \pm 0.05$. Expanding the fit to include the exponents of T_c and σ_{LS} revealed little change in the σ_{LS} exponent, a small increase in the T_c exponent from 1.5 to 1.61 ± 0.13 and even smaller increase in β from 2.93 ± 0.11 to 2.98 ± 0.14 . Regression based on third order polynomials substantially worsened the fit. Our regression analysis suggests $L_T \sim \sigma_{LS}^2 T_c^{-3/2} (\nu_S/\nu_L)^3$, although studies on different systems are needed to finalize these exponents.

IV. CONCLUSION

An extensive NEMD study of 180 systems was conducted to determine how the spatial ordering and vibrational spectrum of the contact layer induced by

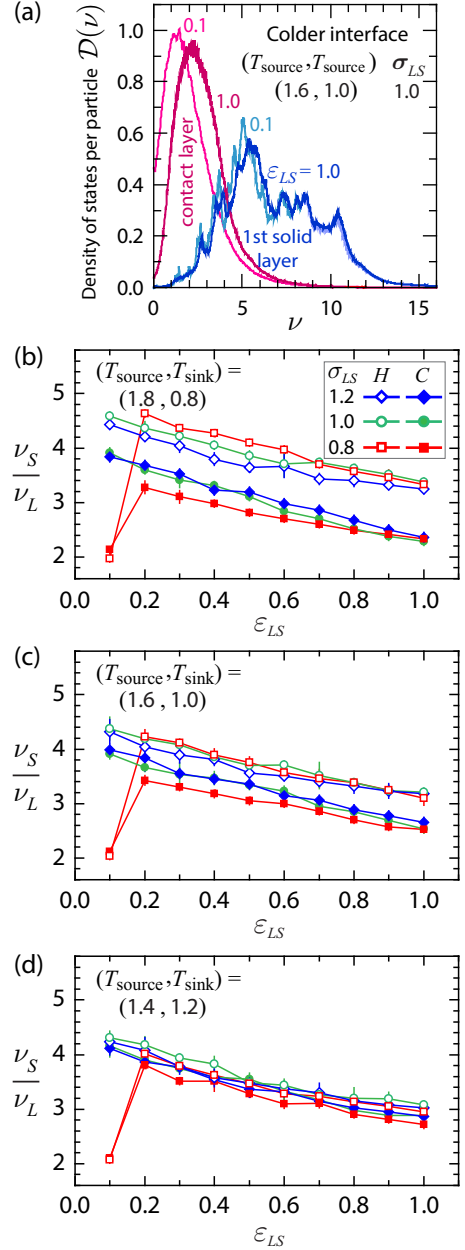


FIG. 5. (a) Per particle frequency spectrum $\mathcal{D}(\nu)$ from Eq. (A.13) for the contact (L) and first solid (S) layer at the colder interface for $(T_{\text{source}}, T_{\text{sink}}) = (1.6, 1.0)$, $\sigma_{LS} = 1.0$ and $\varepsilon_{LS} = 0.1$ and 1.0. (b) - (d) Frequency ratio ν_S/ν_L for 180 systems.

the crystal surface potential regulate the thermal flux crossing the L/S interface. Excluding a handful of cases leading to quasi-solidified contact layers, the data reveal power law relations for quantifying the thermal slip length as a function of the layer temperature, peak magnitude of the in-plane structure factor and ratio of peak vibrational frequency of the contact and first solid layer. These power laws may hold more generally for other systems modeled by Lennard-Jones potentials given the principle of corresponding states [38, 39].

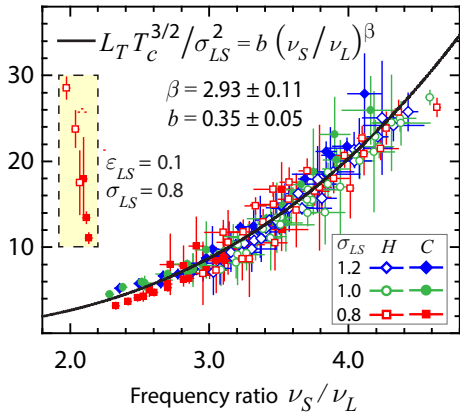


FIG. 6. Rescaled data for 180 systems with best fit to Eq. (5) (solid line) exclusive of six points with $\nu_S/\nu_L \approx 2$.

In addition to guiding optimal experimental designs, these findings offer theorists concrete guidelines for constructing models based on the controlling variables demonstrated. Extending such simulations to other intermolecular potentials will also help establish the universality class of the exponents identified.

ACKNOWLEDGMENTS

The authors gratefully acknowledge funding from a 2019 NASA Space Technology Research Fellowship (HK) and the assistance of Dr. Peter Thompson, IT administrator of the LIS2T computing cluster used in this work.

APPENDIX

This section describes the details of the non-equilibrium molecular dynamics simulations conducted with the software package LAMMPS [40, 41]. All data in support of the findings can be found in Tables III through XI.

1. Methods

The computational study was based on the layered geometry in Fig. 7(a) consisting of a simple liquid sandwiched between the [001] facet plane of a face-centered cubic (FCC) crystal. Each crystal was placed in contact with a thicker FCC crystal acting as a Langevin thermostat fixed to the set point temperatures $(T_{\text{source}}, T_{\text{sink}}) = (1.8, 0.8), (1.6, 1.0)$ or $(1.4, 1.2)$. Particles in the liquid (L) and solid (S) layers, of mass one (in reduced units) such that the mass and number density are equivalent, were made to interact through a truncated and shifted Lennard-Jones (LJ) potential of the form

$$U_{ij}(r) = \begin{cases} U(r) - U(r_c) & \text{if } r \leq r_c , \\ 0 & \text{if } r > r_c \end{cases} \quad (\text{A.6})$$

where

$$U(r) = 4\varepsilon_{ij} \left[\left(\frac{\sigma_{ij}}{r} \right)^{12} - \left(\frac{\sigma_{ij}}{r} \right)^6 \right], \quad (\text{A.7})$$

where subscripts i, j denote L/L, S/S or L/S interactions, $r = |\vec{r}| = (x^2 + y^2 + z^2)^{1/2}$ is the particle separation distance, ε_{ij} is the pairwise interaction energy, σ_{ij} is the pairwise separation distance where $U(r = \sigma_{ij}) = 0$ and the cutoff radius $r_c = 2.5$. The use of the shifted and truncated LJ potential ensured no discontinuity in the force field and therefore no spurious impulsive effects which might otherwise influence the motion. The value σ_{ij} was either 0.8, 1.0 or 1.2; ε_{LS} ranged from 0.1, 0.2, ..., 0.9, 1.0 thereby spanning non-wetting to completely wetting behavior. Scaling variables and parameter values for this study are listed in Table I. The dimensions of the overall cell and layer thicknesses are listed in Table II.

The system was constructed as follows. Initially, the thermostat temperatures were set to identical values $(T_{\text{source}}, T_{\text{sink}}) = (1.3, 1.3)$. The density of the liquid layer was then fixed by situating particles on the sites of the FCC lattice and sequentially removing some until the density of the interior liquid was $\rho_{\text{bulk}} \approx 0.84$ at $T = 1.3$. In this study, the values listed in Table I for the choices $(T_{\text{source}}, T_{\text{sink}})$ ensured that the average temperature of the liquid interior remained at $T = 1.3$, corresponding to a dense bulk fluid far from any critical or triple point [30, 31].

Regarding the construction of the solid layers, the majority of NEMD studies often rely on the so-called harmonic wall-spring model in which solid wall particles are

tethered to fixed crystal lattice sites by a strong Hookean force [26, 42]. Depending on parameter values, the resulting solid can dampen or altogether eliminate anharmonic response of the crystal. The solid regions in this study were instead constructed using a strong-binding LJ potential, a choice which has been demonstrated to yield accurate values of mechanical and interfacial properties of FCC metals [39]. Given also that the melting temperature of an LJ solid is estimated to be $T_m \simeq \varepsilon_{SS}/2$ [43], the choice $\varepsilon_{SS} = 10$ ensured the crystal remained in the solid state for the temperature pairs $(T_{\text{source}}, T_{\text{sink}})$ selected.

The thickness of the solid thermostat layers was selected to exceed the length of the estimated phonon mean free path Λ to avoid inaccurate reduction in the value of TBR [44]. Studies have shown that for $\Lambda = c_\ell \times \tau_{\text{damp}} \leq 2L$, where c_ℓ is the speed of longitudinal sound waves [20] and L the layer thickness, phonons are dissipated before undergoing reflection and propagation from the exterior boundary to the L/S interface. For an FCC crystal, the speed c_ℓ can be approximated [43] by the relation $c_\ell = 9.53\sqrt{\varepsilon_{SS}}$. For the parameter values in our study, namely $\varepsilon_{SS} = 10$, $\tau_{\text{damp}} = 1$ and $L_s = L^{\text{source}} = L^{\text{sink}} = 39$, the inequality $\Lambda = c_\ell \times \tau_{\text{damp}} = 9.53\sqrt{10} \simeq 30 \leq 2L_s = 78$ was satisfied.

Periodic boundary conditions were enforced along the \hat{x} and \hat{y} axes. Trajectories of particles were computed using second order Verlet integration [45] based on a time step Δt_{int} . The system was first equilibrated with a Nosé–Hoover thermostat [46] set to $T_{NH} = 1.3$ for a period $t_{eq} = 10^5 \Delta t_{\text{int}} = 200$ to establish an NVT ensemble. This thermostat was then switched off and the motion of particles within the solid thermal source and sink regions

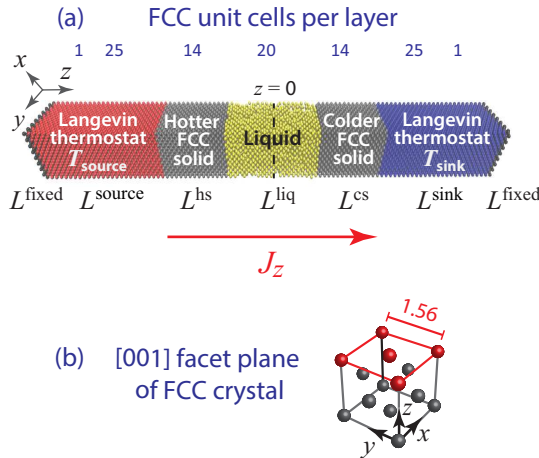


FIG. 7. (a) Rectangular geometry showing layered structure with number of FCC unit cell lengths per layer exposed to thermal source and sink temperatures ($T_{\text{source}}, T_{\text{sink}}$) enforced by Langevin thermostats. Coordinate origin $z = 0$ is situated at the central plane of the liquid layer. (b) Lattice sites of [001] facet plane (red) for FCC crystal with edge length $a^* = 1.560\sigma^*$.

[see Fig. 7(a)] controlled by a Langevin thermostat enforced by [47]

$$\frac{d^2\vec{r}_i}{dt^2} = -\sum_{i \neq j} \frac{dU_{ij}(r)}{dr} \hat{r}_i - \frac{1}{\tau_{\text{damp}}} \frac{d\vec{r}_i}{dt} + \vec{F}_{\text{stoch}}, \quad (\text{A.8})$$

where \vec{r}_i is the 3D coordinate of particle i , $\tau_{\text{damp}} = 500 \Delta t_{\text{int}} = 1.0$ is the damping constant, \vec{F}_{stoch} is a random force vector representing a normal distribution of magnitude $[T_s / (\tau_{\text{damp}} \Delta t_{\text{int}})]^{1/2}$ and the temperatures T_s of the source and sink pair set to $(T_{\text{source}}, T_{\text{sink}} = (1.8, 0.8), (1.6, 1.0)$ or $(1.4, 1.2)$. During this period, the system was stabilized for an additional time $2 \times 10^5 \Delta t_{\text{int}} = 400$ to ensure steady state conditions before measurement.

The thermal flux was then computed from the relation

$$J_z = \frac{1}{L_x \times L_y} \left\langle \frac{E_{\text{net}}(t)}{t} \right\rangle, \quad (\text{A.9})$$

where $E_{\text{net}}(t)$ is the net energy input over the interval t needed to maintain the set point temperatures. The angular brackets denote the ensemble average, as described in the following section. It was confirmed that $\langle E_{\text{net}}(t) \rangle$ increased linearly in time, as required at steady state. The mean and standard deviation for $|dT/dz|$ were extracted from least squares fits over the linear portion of the temperature distribution within the interior liquid and solid layers. The values of the thermal conductivity k in Tables III – V, extracted from the ratio $k = J_z / |dT/dz|$, were not used in any of the analysis but are only provided for reference.

The virial contribution to the pressure within the interior of the liquid layer was confirmed to depend only weakly on ε_{LS} . Specifically, the virial contribution to the pressure for $\sigma_{LS} = 1.0$ at $\varepsilon_{LS} = 0.1$ was 2.72 ± 0.03 and at $\varepsilon_{LS} = 1.0$ was 2.54 ± 0.02 . Since the interior liquid temperature remained close to $T = 1.3$ for all runs conducted, the kinetic contribution to the liquid pressure (roughly 1.5) remained rather constant. Relative to other factors discussed in the main article, the bulk liquid pressure did not contribute in any significant way to measured reductions in the thermal slip length, this in agreement with other studies demonstrating that much higher pressures are needed to cause a reduction in the thermal boundary resistance [20].

For each set of input parameters, measurements were extracted from the hotter and colder L/S interface to discern the influence of the contact layer temperature T_c as well. These measurements included the contact layer density ρ_c , density depletion layer thickness δ_{LS} , interface temperature drop Δ , thermal slip length L_T , peak value of the in-plane static structure factor of the contact layer S_{max} and the peak frequencies ν_L and ν_S characterizing the maximum value of the density of states $\mathcal{D}(\nu)$ for particles in the contact layer (L) and first solid (S) layer.

Physical quantity	Numerical value
mass	$m^* = 6.690 \times 10^{-26}$ kg
length	$\sigma^* = 0.3405 \times 10^{-9}$ m
energy	$\epsilon^* = 165.3 \times 10^{-23}$ J
temperature	$T^* = \epsilon^*/k_B = 119.8$ °K
time	$t^* = (m^*\sigma^{*2}/\epsilon^*)^{1/2} = 2.14$ ps
mass density	$\rho^* = m^*/(\sigma^*)^3$
pressure	$p^* = \epsilon^*/(\sigma^*)^3 = 0.4187$ MPa
effective particle diameters	$\sigma_{LL}^* = \sigma_{LS}^* = \sigma_{SS}^* = \sigma^*$
FCC edge length	$a^* = 1.560 \sigma^* = 5.312 \times 10^{-10}$ m
interaction energies	$\epsilon_{LL} = \epsilon^*$ $\epsilon_{LS} = 0.1 - 1.0 \epsilon^*$ $\epsilon_{SS} = 10 \epsilon^*$
Variable	Value in scaled units
solid & liquid particle mass	1.0
LJ repulsive distances	$\sigma_{LL} = \sigma_{SS} = 1.0$ $\sigma_{LS} = 0.8, 1.0$ or 1.2
FCC edge length	$a = 1.560$
integration time step	$\Delta t_{int} = 0.002$
Thermostat set points	$(T_{source}, T_{sink}) = (1.8, 0.8), (1.6, 1.0)$ or $(1.4, 1.2)$
LJ interaction energy	$\epsilon_{LL} = 1.0$ $\epsilon_{LS} = 0.1, 0.2, \dots, 0.9, 1.0$ $\epsilon_{SS} = 10$
bulk liquid density	$\rho_L \approx 0.84$
FCC unit cell density	$\rho_S = 1.0536$

TABLE I. Symbols, numerical values and scalings for non-dimensionalization of physical quantities based on fluid argon [30, 45, 48]. Asterisk superscripts denote dimensional units. Boltzmann's constant $k_B = 1.380649 \times 10^{-23}$ J/K.

Cell sizes (scaled by σ^*)	FCC [001]
L_x	12.48
L_y	12.48
L^{fixed} (1 unit cell per end)	1.56
L^{source}	39.00
L^{hs}	21.84
L^{liq}	31.20
L^{cs}	21.84
L^{sink}	39.00
Total length along z axis	156.00

TABLE II. Dimensions of multilayer geometry in Fig. 7.

2. Averaging procedure for time-independent quantities

After steady state was established, simulations were carried out for a total run time $t_{\text{total}} = 5 \times 10^6 \Delta t_{int} = 10^4$. For measurements of time-independent quantities, these data was divided into ten equal and non-overlapping segments, representing ten ensembles extending a period 10^3 with data sampled at a rate $500 \Delta t_{int} = 1.0$. This rate corresponded to the typical time for the velocity auto-correlation function to decay to zero. Angular brackets $\langle \cdot \rangle$ signify the mean with standard deviation computed from the average value of the ten ensembles.

The spatial variation in density and temperature along the \hat{z} axis was obtained by partitioning the liquid and solid layers into non-overlapping bins of area $L_x \times L_y$ and width Δz_{bin} . To ensure sufficient resolution for capturing the rapidly decaying oscillations in liquid density near the L/S interface, the bin width for density measurements was set to a finer width $\Delta z_{\text{bin}} = 0.016$. The local density within an individual bin was estimated from $\rho_{\text{bin}} = \langle N_{\text{bin}} \rangle / V_{\text{bin}}$ where $\langle N_{\text{bin}} \rangle$ is the average number of particles in a single bin of volume $V_{\text{bin}} = L_x \times L_y \times 0.016 = 2.49$.

In this work, the *contact layer* denotes those set of particles in the first liquid layer adjacent to the solid surface. The thickness of this layer was measured to be the distance between neighboring minima of $\rho(z)$ of the first oscillation in the liquid density, whose peak value defines the so-called contact density ρ_c .

Measurements of particle speeds at steady state in the contact and first solid layer confirmed Maxwell-Boltzmann statistics such that layer temperatures could be extracted directly from the equipartition relation. The temperature $T(z)$ within the solid and liquid layers, obtained with a coarser bin width $\Delta z_{\text{bin}} = 0.785$, was estimated from the average bin temperatures

$$T_{\text{bin}} = \left\langle \frac{1}{3 N_{\text{bin}}} \sum_i^{N_{\text{bin}}} \mathbf{v}_i^2 \right\rangle, \quad (\text{A.10})$$

where \mathbf{v} denotes the 3D velocity. Too small a bin width caused excessively noisy velocity and thermal profiles from large fluctuations in N_{bin} . It was confirmed that even for the finer bin width $\Delta z_{\text{bin}} = 0.016$, $\langle T(z) \rangle$ did not exhibit oscillations near the L/S interface, as anticipated since T_{bin} is normalized by the factor N_{bin} , unlike the expression for ρ_{bin} .

The interface temperature drop ΔT was computed by extrapolating the linear temperature profiles within the interior regions of the liquid and adjacent solid layer toward the L/S interface and evaluating the temperature jump at the midpoint of the distance separating the location of the peak solid density and that of the contact density. The thermal slip length was then evaluated from

the relation

$$L_T = \left\langle \frac{\Delta T}{|dT/dz|_{lia}} \right\rangle, \quad (\text{A.11})$$

where $|dT/dz|_{lia}$ is the magnitude of the thermal gradient in the liquid interior away from either L/S interface. With all parameter values fixed, the thermal slip lengths evaluated from Eq. (A.11) at the hotter and colder interface therefore differed in magnitude.

Long range translational order within the contact (c) layer was quantified by the static in-plane structure factor normalized to $0 \leq S_c^{\parallel}(\mathbf{k}) \leq 1$ and given by

$$S_c^{\parallel}(\vec{k}) = \left\langle \frac{1}{N_c^2} \sum_{p=1}^{N_c} \sum_{q=1}^{N_c} \exp [i\mathbf{k} \cdot (\mathbf{r}_p - \mathbf{r}_q)] \right\rangle, \quad (\text{A.12})$$

where the superscript \parallel denotes the 2D structure factor based on planar coordinates $\mathbf{r} = (x, y)$ and wave numbers $\mathbf{k} = (k_x, k_y)$. Here, N_c is the number of particles in the contact layer and the angular brackets denote the ten ensemble average. For the parameter values in this study, the maxima S_{\max} evaluated from Eq. (A.12) always coincided with the smallest reciprocal lattice vectors $\mathbf{k}_o = (\pm 4.03, \pm 4.03)$ or $(\mp 4.03, \pm 4.03)$ of the FCC [001] facet plane of a unit cell with edge length 1.56. It was confirmed that contributions from the imaginary parts of Eq. (A.12) were negligible.

3. Averaging procedure for time-dependent quantities

For evaluation of the time-dependent velocity auto-correlation function, data was collected over an interval $t_{\text{total}} = 1.5 \times 10^6 \Delta t_{int} = 3 \times 10^3$ divided into three equal and non-overlapping blocks initialized at $t_o^B = 0, 10^3$ and 2×10^3 . Particle velocities in each of these blocks were sampled every ten time steps ($10\Delta t_{int} = 0.02$) thereby generating a sequence of velocity autocorrelations extending in time from $t_o = t_o^B + (0, 10, 20, \dots, 475, 000) \times \Delta t_{int}$ to t_f .

Since particles in the solid remained in very close proximity to the sites of the [001] FCC lattice, the termination time was simply set to $t_f = 50$. For the contact layer, a different strategy was required since the velocity autocorrelation requires information about the same particle at different times. However, liquid particles in the contact layer often exit the layer, some to return and some not. For this study therefore, evaluation of the velocity auto-correlation function was restricted to those trajectories of ten or more particles which remained within the layer for the specified measurement period, never having escaped. Data collection spanned the period $t_o \leq t \leq t_o + t_f$ where t_f was the time at which ten or more particles from the original set of occupants at t_o still remained. In all cases, t_f exceeded the decay time of the velocity autocorrelation function by at least an order of magnitude. Since each start time t_o yielded different values t_f , the short-

est time t_f within a block was used to estimate averages for that block and the shortest time t_f over all three blocks then used to compute the final block (B) average. Fourier transforms of the velocity auto-correlation were statistically averaged to obtain a single distribution $\mathcal{D}(\nu)$ from Eq. (A.13) for each block and the three-block average of $\mathcal{D}(\nu)$ computed to yield the final mean value with standard deviation. The symbol $\langle \cdot \rangle_{t_o}^B$ signifies the ensemble average over initialization times t_o followed by the three-block average.

The density of states per particle $\mathcal{D}(\nu)$ for the contact layer and first solid layer, representing the normal mode vibrational spectrum, was computed from the relation [33, 34]

$$\mathcal{D}(\nu) = \left\langle \frac{4}{N_L T_L} \int_0^{t_f} \sum_{j=1}^{N_L} \mathbf{v}_j(t_o+t) \cdot \mathbf{v}_j(t_o) \cos(2\pi i \nu t) dt \right\rangle_{t_o}^B, \quad (\text{A.13})$$

normalized to satisfy $\int_0^\infty \mathcal{D}(\nu) d\nu = 3$ in accord with the equipartition theorem. Here, $\mathbf{v} = (v_x, v_y, v_z)$, T_L is the average temperature of the layer and $N_L = N_L(t_o, t_f)$ is the number of initial particles in the layer at t_o which remained there through t_f , never having exited. For the contact layer, the constraint imposed was $N_L = N_L(t_o, t_f) \geq 10$. It was confirmed that contributions from the imaginary part of Eq. (A.13) proportional to $\sin(2\pi i \nu t)$ (not shown) were negligible.

-
- [1] R. van Erp, R. Soleimanzadeh, L. Nela, G. Kampitis, and E. Matioli, Co-designing electronics with microfluidics for more sustainable cooling, *Nature* **585**, 211 (2020).
- [2] G. Rak, IBM demos transistor built for liquid nitrogen cooling, <https://spectrum.ieee.org/nanosheet-transistor> (2023).
- [3] S. Rangarajan, S. N. Schiffres, and B. Sammakia, A review of recent developments in “on-chip” embedded cooling technologies for heterogeneous integrated applications, *Engineering* **26**, 185 (2023).
- [4] R. Saligram, A. Raychowdhury, and S. Datta, The future is frozen: cryogenic CMOS for high-performance computing, *Chip* **3**, 100082 (2024).
- [5] I. M. Khalatnikov, Teploobmen mezhdu tverdym telom i Geliem-ii, *Zh. Eksp. Teor. Fiz.* **22**, 687 (1952).
- [6] E. T. Swartz and R. O. Pohl, Thermal boundary resistance, *Rev. Mod. Phys.* **61**, 605 (1989).
- [7] G. L. Pollack, Kapitza resistance, *Rev. Mod. Phys.* **41**, 48 (1969).
- [8] P. A. Thompson and S. M. Troian, A general boundary condition for liquid flow at solid surfaces, *Nature* **389**, 360 (1997).
- [9] J.-L. Barrat and L. Bocquet, Influence of wetting properties on hydrodynamic boundary conditions at a fluid/solid interface, *Faraday Discuss.* **112**, 119 (1999).
- [10] N. V. Priezjev and S. M. Troian, Molecular origin and dynamic behavior of slip in sheared polymer films, *Phys. Rev. Lett.* **92**, 018302 (2004).
- [11] N. V. Priezjev, A. A. Darhuber, and S. M. Troian, Slip behavior in liquid films on surfaces of patterned wettability: Comparison between continuum and molecular dynamics, *Phys. Rev. E* **71**, 041608 (2005).
- [12] N. V. Priezjev and S. M. Troian, Influence of periodic wall roughness on the slip behaviour at liquid/solid interfaces: molecular-scale simulations versus continuum predictions, *J. Fluid Mech.* **554**, 24 (2006).
- [13] S. Matsumoto, Molecular dynamics simulation of a liquid droplet on a solid surface, *J. Jap. Soc. Tribologists* **42**, 93 (1997).
- [14] S. Maruyama, T. Kurashige, S. Matsumoto, Y. Yamaguchi, and T. Kimura, Liquid droplet in contact with a solid surface, *Micro. Thermophys. Eng.* **2**, 49 (1998).
- [15] T. Ohara and D. Suzuki, Intermolecular energy transfer at a solid–liquid interface, *Micro. Thermophys. Eng.* **4**, 189 (2000).
- [16] J.-L. Barrat and F. Chiaruttini, Kapitza resistance at the liquid–solid interface, *Mol. Phys.* **101**, 1605 (2003).
- [17] L. Xue, P. Kebinski, S. R. Phillpot, S. U.-S. Choi, and J. A. Eastman, Two regimes of thermal resistance at a liquid–solid interface, *J. Chem. Phys.* **118**, 337 (2003).
- [18] M. Vuorio, Role of wetting and nanoscale roughness on thermal conductance at liquid–solid interface, *Appl. Phys. Lett.* **99**, 073112 (2011).
- [19] S. Murad and I. K. Puri, Thermal transport across nanoscale solid–fluid interfaces, *Appl. Phys. Lett.* **92**, 133105 (2008).
- [20] H. Han, S. Mérabia, and F. Müller-Plathe, Thermal transport at solid–liquid interfaces: High pressure facilitates heat flow through nonlocal liquid structuring, *J. Phys. Chem. Lett.* **8**, 1946 (2017).
- [21] G. Balasubramanian, S. Banerjee, and I. K. Puri, Unsteady nanoscale thermal transport across a solid–fluid interface, *J. Appl. Phys.* **104**, 064306 (2008).
- [22] A. K. M. M. Morshed, T. Paul, and J. A. Khan, Atomistic simulation of temperature dependent thermal transport across nanoconfined liquid, *Physica E* **47**, 246 (2013).
- [23] T. Ohara and D. Torii, Molecular dynamics study of thermal phenomena in an ultrathin liquid film sheared between solid surfaces: The influence of the crystal plane on energy and momentum transfer at solid–liquid interfaces, *J. Chem. Phys.* **122**, 214717 (2005).
- [24] D. Torii, T. Ohara, and K. Ishida, Molecular-scale mechanism of thermal resistance at the solid–liquid interfaces: Influence of interaction parameters between solid and liquid molecules, *J. Heat Transfer* **132**, 012402 (2010).
- [25] H. Kaifu, S. M. Troian, and A. I. Baskin, How caged motion in the contact layer enhances thermal tunneling across a liquid/solid interface, *Phys. Rev. Research* **6**, 033123 (2024).
- [26] B. H. Kim, A. Beskok, and T. Cagin, Molecular dynamics simulations of thermal resistance at the liquid–solid interface, *J. Chem. Phys.* **129**, 174701 (2008).
- [27] B. Ramos-Alvarado, S. Kumar, and G. P. Peterson, Solid–liquid thermal transport and its relationship with wettability and the interfacial liquid structure, *J. Phys. Chem. Lett.* **7**, 3497 (2016).
- [28] C. U. Gonzalez-Valle, S. Kumar, and B. Ramos-Alvarado, Thermal transport across SiC–water interfaces, *ACS Appl. Mater. Interfaces* **10**, 29179 (2018).
- [29] S. Li, Y. Chen, J. Zhao, C. Wang, and N. Wei, Atomic structure causing an obvious difference in thermal conductance at the Pd–H₂O interface: A molecular dynamics simulation, *Nanoscale* **12**, 17870 (2020).
- [30] B. L. Holian and D. J. Evans, Shear viscosities away from the melting line: A comparison of equilibrium and nonequilibrium molecular dynamics, *J. Chem. Phys.* **78**, 5147 (1983).
- [31] M. Thol, G. Rutkai, A. Köster, R. Lustig, R. Span, and J. Vrabec, Equation of state for the Lennard-Jones fluid, *J. Phys. Chem. Ref. Data* **45**, 023101 (2016).
- [32] In many studies of the L/S interface, the liquid structure factor is often computed from the relation $|\sum_p^{N_c} \exp(-ik \cdot r_p)|^2$, a simplification strictly valid for particles on sites of a Bravais lattice.
- [33] P. H. Berens, D. H. J. Mackay, G. M. White, and K. R. Wilson, Thermodynamics and quantum corrections from molecular dynamics for liquid water, *J. Chem. Phys.* **79**, 2375 (1983).
- [34] S. T. Lin, M. Blanco, and W. A. Goddard, The two-phase model for calculating thermodynamic properties of liquids from molecular dynamics: Validation for the phase diagram of Lennard-Jones fluids, *J. Chem. Phys.* **119**, 11792 (2003).
- [35] S. Murad and I. K. Puri, Molecular simulation of thermal transport across hydrophilic interfaces, *Chem. Phys. Lett.* **467**, 110 (2008).
- [36] A. Pham, M. Barisik, and B. Kim, Pressure dependence of Kapitza resistance at gold/water and silicon/water interfaces, *J. Chem. Phys.* **139**, 244702 (2013).
- [37] P. A. Thompson and M. O. Robbins, Shear flow near solids: Epitaxial reader and flow boundary conditions,

TABLE III. Mean and standard deviation (in parenthesis) for the thermal flux J_z and magnitude of the thermal gradient $|dT/dz|$ in the interior liquid and solid layers for $(T_{\text{source}}, T_{\text{sink}}) = (1.8, 0.8)$, $\sigma_{LS} = 0.8, 1.0$ and 1.2 and $\varepsilon_{LS} = 0.1, 0.2, \dots, 0.9, 1.0$. All quantities are in reduced units given in Table I. (Entries must be multiplied by the numerical factor in the column heading).

σ_{LS}	ε_{LS}	$J_z \times 10^{-2}$	Liquid layer		Hotter solid layer		Colder solid layer	
			$ dT/dz \times 10^{-2}$	k	$ dT/dz \times 10^{-4}$	$k \times 10^2$	$ dT/dz \times 10^{-4}$	$k \times 10^2$
0.8	0.1	13.74(0.05)	1.99(0.03)	6.93(0.10)	9.29(1.98)	1.52(0.37)	4.85(0.69)	2.86(0.44)
0.8	0.2	14.15(0.06)	2.04(0.03)	6.94(0.11)	9.89(1.89)	1.52(0.35)	4.95(0.73)	2.88(0.44)
0.8	0.3	14.55(0.08)	2.09(0.03)	6.95(0.10)	8.11(1.53)	1.81(0.32)	4.55(0.73)	3.18(0.44)
0.8	0.4	15.06(0.09)	2.15(0.03)	6.99(0.10)	9.34(1.58)	1.69(0.29)	4.58(0.93)	3.41(0.77)
0.8	0.5	15.26(0.08)	2.20(0.03)	6.92(0.11)	10.42(1.30)	1.51(0.19)	4.27(1.16)	3.56(0.87)
0.8	0.6	15.67(0.05)	2.28(0.02)	6.89(0.07)	10.08(2.06)	1.60(0.40)	5.19(1.01)	2.93(0.39)
0.8	0.7	15.94(0.04)	2.32(0.02)	6.89(0.07)	11.45(1.99)	1.47(0.29)	5.46(0.81)	3.03(0.39)
0.8	0.8	16.34(0.09)	2.37(0.03)	6.90(0.09)	10.86(1.85)	1.55(0.28)	5.36(1.09)	2.99(0.45)
0.8	0.9	16.33(0.06)	2.40(0.02)	6.80(0.07)	11.05(2.54)	1.54(0.32)	5.02(0.94)	3.48(0.85)
0.8	1.0	16.62(0.03)	2.46(0.02)	6.75(0.06)	9.98(1.18)	1.67(0.19)	5.58(1.08)	3.12(0.72)
1.0	0.1	11.26(0.05)	1.54(0.01)	7.30(0.07)	7.57(2.19)	1.57(0.47)	4.01(0.40)	2.87(0.30)
1.0	0.2	12.06(0.03)	1.63(0.04)	7.42(0.17)	8.14(1.18)	1.53(0.25)	4.42(0.94)	2.92(0.53)
1.0	0.3	12.87(0.04)	1.75(0.03)	7.38(0.12)	8.71(1.85)	1.55(0.32)	4.76(0.83)	2.79(0.70)
1.0	0.4	13.29(0.08)	1.82(0.02)	7.32(0.11)	9.14(2.15)	1.48(0.36)	4.59(0.92)	3.08(0.66)
1.0	0.5	14.06(0.05)	1.91(0.03)	7.37(0.11)	8.15(1.07)	1.77(0.25)	5.31(1.07)	2.74(0.63)
1.0	0.6	14.49(0.04)	2.00(0.02)	7.27(0.06)	9.61(2.25)	1.60(0.51)	5.38(0.96)	2.80(0.58)
1.0	0.7	14.94(0.05)	2.06(0.03)	7.26(0.09)	10.76(2.95)	1.39(0.34)	5.23(0.97)	2.99(0.66)
1.0	0.8	15.35(0.05)	2.12(0.02)	7.25(0.05)	9.76(1.34)	1.61(0.24)	5.61(0.68)	2.79(0.42)
1.0	0.9	15.71(0.05)	2.17(0.02)	7.23(0.05)	10.94(0.90)	1.44(0.12)	5.46(0.67)	2.92(0.40)
1.0	1.0	15.94(0.10)	2.25(0.03)	7.09(0.10)	9.68(2.07)	1.77(0.45)	5.32(1.11)	3.07(0.74)
1.2	0.1	9.72(0.10)	1.28(0.05)	7.60(0.24)	6.23(1.51)	1.69(0.67)	3.64(0.93)	2.88(1.00)
1.2	0.2	10.79(0.06)	1.37(0.02)	7.83(0.14)	6.58(1.54)	1.75(0.56)	4.20(0.72)	2.67(0.45)
1.2	0.3	11.48(0.04)	1.49(0.02)	7.70(0.10)	7.24(2.15)	1.72(0.55)	3.90(0.82)	3.10(0.82)
1.2	0.4	12.28(0.01)	1.60(0.02)	7.64(0.08)	8.64(0.87)	1.44(0.16)	3.96(1.02)	3.39(0.78)
1.2	0.5	12.86(0.04)	1.69(0.02)	7.64(0.11)	8.23(1.92)	1.62(0.44)	4.68(0.68)	2.85(0.48)
1.2	0.6	13.50(0.06)	1.79(0.02)	7.55(0.10)	8.41(1.74)	1.71(0.41)	4.62(1.43)	3.30(0.88)
1.2	0.7	13.99(0.09)	1.87(0.03)	7.49(0.16)	9.15(2.17)	1.66(0.45)	5.05(0.46)	2.79(0.27)
1.2	0.8	14.66(0.04)	1.94(0.03)	7.52(0.14)	10.52(1.64)	1.42(0.29)	5.32(0.72)	2.86(0.44)
1.2	0.9	15.05(0.06)	2.01(0.02)	7.49(0.06)	9.48(1.23)	1.64(0.20)	5.27(0.97)	3.03(0.52)
1.2	1.0	15.44(0.04)	2.06(0.03)	7.48(0.11)	9.33(1.92)	1.78(0.29)	5.01(0.95)	3.06(0.52)

- Phys. Rev. A **41**, 6830 (1990).
- [38] E. Helfand and S. A. Rice, Principle of corresponding states for transport properties, J. Chem. Phys. **32**, 1642 (1960).
- [39] K. Kanhaiya, S. Kim, W. Im, and H. Heinz, Accurate simulation of surfaces and interfaces of ten FCC metals and steel using Lennard-Jones potentials, NPJ Comput. Mater. **7**, 17 (2021).
- [40] S. Plimpton, Fast parallel algorithms for short-range molecular dynamics, J. Comput. Phys. **117**, 1 (1995).
- [41] A. P. Thompson, H. M. Aktulga, R. Berger, D. S. Bolintineanu, W. M. Brown, P. S. Crozier, P. J. intVelde, A. Kohlmeyer, S. G. Moore, T. D. Nguyen, R. Shan, M. J. Stevens, J. Tranchida, C. Trott, and S. J. Plimpton, LAMMPS – A flexible simulation tool for particle-based materials modeling at the atomic, meso, and continuum scales, Comp. Phys. Comm. **271**, 108171 (2022).
- [42] M. Cieplak, J. Koplik, and J. R. Banavar, Boundary conditions at a fluid–solid interface, Phys. Rev. Lett. **86**, 803 (2001).
- [43] R. J. Stevens, L. V. Zhigilei, and P. M. Norris, Effects of temperature and disorder on thermal boundary conductance at solid–solid interfaces: Nonequilibrium molecular dynamics simulations, Int. J. Mech. Sci. **50**, 3977 (2007).
- [44] Z. Liang and P. Kebinski, Finite-size effects on molecular dynamics interfacial thermal-resistance predictions, Phys. Rev. B **90**, 075411 (2014).
- [45] L. Verlet, Computer “experiments” on classical fluids. i. Thermodynamical properties of Lennard-Jones molecules, Phys. Rev. **159**, 98 (1967).
- [46] W. G. Hoover, Canonical dynamics: Equilibrium phase-space distributions, Phys. Rev. A **31**, 1695 (1985).
- [47] T. Schneider and E. Stoll, Molecular-dynamics study of a three-dimensional one-component model for distortive

TABLE IV. Mean and standard deviation (in parenthesis) for the thermal flux J_z and magnitude of the thermal gradient $|dT/dz|$ in the interior liquid and solid layers for $(T_{\text{source}}, T_{\text{sink}}) = (1.6, 1.0)$, $\sigma_{LS} = 0.8, 1.0$ and 1.2 and $\varepsilon_{LS} = 0.1, 0.2, \dots, 0.9, 1.0$. All quantities are in reduced units given in Table I. (Entries must be multiplied by the numerical factor in the column heading).

σ_{LS}	ε_{LS}	$J_z \times 10^{-2}$	Liquid layer		Hotter solid layer		Colder solid layer	
			$ dT/dz \times 10^{-2}$	k	$ dT/dz \times 10^{-4}$	$k \times 10^2$	$ dT/dz \times 10^{-4}$	$k \times 10^2$
0.8	0.1	8.35(0.05)	1.21(0.03)	6.92(0.14)	4.74(1.61)	1.86(0.66)	3.44(0.85)	2.52(0.62)
0.8	0.2	8.59(0.03)	1.24(0.02)	6.91(0.11)	4.52(1.12)	2.13(0.80)	3.14(0.86)	3.09(1.43)
0.8	0.3	8.84(0.03)	1.27(0.03)	7.01(0.17)	5.56(1.28)	1.58(0.32)	3.89(1.65)	2.29(0.86)
0.8	0.4	9.12(0.02)	1.32(0.02)	6.94(0.12)	5.66(1.66)	1.79(0.60)	3.81(1.04)	2.55(0.85)
0.8	0.5	9.55(0.02)	1.35(0.03)	7.12(0.12)	6.03(1.78)	1.73(0.49)	4.05(1.26)	2.50(1.15)
0.8	0.6	9.54(0.06)	1.38(0.02)	6.89(0.13)	5.44(1.41)	1.93(0.65)	3.62(0.88)	2.83(0.68)
0.8	0.7	9.76(0.03)	1.40(0.03)	6.97(0.16)	5.11(2.42)	2.48(1.96)	4.11(1.10)	2.48(0.75)
0.8	0.8	9.96(0.03)	1.44(0.02)	6.95(0.10)	6.26(1.92)	1.68(0.48)	4.27(0.77)	2.44(0.50)
0.8	0.9	10.02(0.08)	1.47(0.02)	6.81(0.11)	5.51(1.37)	1.84(0.41)	3.84(1.30)	3.04(1.06)
0.8	1.0	10.02(0.04)	1.48(0.02)	6.77(0.11)	5.95(1.94)	1.98(0.72)	4.53(1.38)	2.67(1.53)
1.0	0.1	6.91(0.08)	0.94(0.03)	7.38(0.24)	4.54(1.58)	1.89(1.00)	2.87(0.97)	2.49(0.94)
1.0	0.2	7.19(0.03)	0.99(0.02)	7.29(0.16)	4.68(1.81)	1.95(1.05)	3.20(0.84)	2.44(0.53)
1.0	0.3	7.84(0.03)	1.05(0.04)	7.46(0.30)	4.41(2.15)	2.14(1.15)	3.58(1.10)	2.27(0.71)
1.0	0.4	8.14(0.02)	1.10(0.03)	7.39(0.18)	4.92(1.97)	1.83(0.73)	3.48(1.66)	2.56(1.33)
1.0	0.5	8.60(0.03)	1.17(0.03)	7.35(0.19)	4.31(1.15)	2.14(0.65)	3.42(0.67)	2.61(0.54)
1.0	0.6	8.82(0.05)	1.22(0.03)	7.27(0.19)	4.87(2.04)	2.38(1.47)	3.27(1.34)	2.77(1.10)
1.0	0.7	9.21(0.07)	1.27(0.03)	7.28(0.25)	5.22(1.69)	2.06(0.76)	3.60(1.33)	2.74(1.18)
1.0	0.8	9.34(0.07)	1.29(0.03)	7.24(0.15)	5.21(1.59)	1.92(0.94)	3.32(1.08)	2.84(0.85)
1.0	0.9	9.62(0.05)	1.33(0.02)	7.25(0.13)	5.64(1.25)	1.75(0.36)	3.95(0.92)	2.51(0.78)
1.0	1.0	9.84(0.05)	1.35(0.03)	7.26(0.15)	6.11(1.64)	1.66(0.43)	3.85(1.34)	3.01(1.62)
1.2	0.1	5.84(0.04)	0.77(0.03)	7.60(0.29)	4.07(1.56)	1.90(1.29)	2.32(0.80)	2.65(0.94)
1.2	0.2	6.53(0.05)	0.83(0.04)	7.88(0.35)	4.06(1.70)	2.14(1.49)	3.06(0.89)	2.19(0.61)
1.2	0.3	6.94(0.09)	0.90(0.03)	7.69(0.25)	3.89(1.16)	2.01(0.98)	2.45(0.92)	3.23(1.09)
1.2	0.4	7.33(0.02)	0.97(0.03)	7.56(0.23)	4.15(2.09)	2.19(1.24)	3.61(0.90)	2.13(0.65)
1.2	0.5	7.79(0.02)	1.02(0.02)	7.67(0.15)	4.56(1.34)	1.86(0.84)	3.60(1.16)	2.49(1.15)
1.2	0.6	8.15(0.03)	1.08(0.02)	7.53(0.14)	5.45(1.94)	2.03(1.72)	3.25(1.65)	3.35(1.48)
1.2	0.7	8.53(0.03)	1.11(0.02)	7.69(0.17)	5.46(1.82)	1.74(0.60)	3.31(0.99)	2.93(0.86)
1.2	0.8	8.81(0.10)	1.17(0.03)	7.53(0.23)	5.30(1.91)	1.87(0.75)	3.59(1.27)	3.43(3.27)
1.2	0.9	9.18(0.05)	1.21(0.02)	7.61(0.15)	6.13(1.17)	1.57(0.37)	3.23(0.61)	2.74(0.34)
1.2	1.0	9.18(0.04)	1.26(0.02)	7.31(0.11)	5.82(1.39)	1.66(0.38)	3.70(0.74)	2.61(0.60)

phase transitions, Phys. Rev. B **17**, 1302 (1978).
[48] A. Michels, H. Wijker, and H. Wijker, Isotherms of ar-

gon between 0°C and 150°C and pressures up to 2900 atmospheres, Physica **XV**, 627 (1949).

TABLE V. Mean and standard deviation (in parenthesis) for the thermal flux J_z and magnitude of the thermal gradient $|dT/dz|$ in the interior liquid and solid layers for $(T_{\text{source}}, T_{\text{sink}}) = (1.4, 1.2)$, $\sigma_{LS} = 0.8, 1.0$ and 1.2 and $\varepsilon_{LS} = 0.1, 0.2, \dots, 0.9, 1.0$. All quantities are in reduced units given in Table I. (Entries must be multiplied by the numerical factor in the column heading).

σ_{LS}	ε_{LS}	$J_z \times 10^{-2}$	Liquid layer		Hotter solid layer		Colder solid layer	
			$ dT/dz \times 10^{-2}$	k	$ dT/dz \times 10^{-4}$	$k \times 10^2$	$ dT/dz \times 10^{-4}$	$k \times 10^2$
0.8	0.1	2.67(0.04)	0.41(0.03)	6.64(0.55)	2.24(1.07)	1.55(0.80)	1.08(0.91)	7.54(8.04)
0.8	0.2	2.89(0.06)	0.42(0.02)	6.93(0.36)	1.46(0.86)	2.49(1.70)	0.99(1.01)	8.58(10.23)
0.8	0.3	2.92(0.04)	0.41(0.04)	7.23(0.59)	1.92(1.50)	3.20(3.41)	1.55(1.30)	4.01(4.66)
0.8	0.4	3.08(0.04)	0.44(0.02)	7.02(0.41)	2.13(1.29)	2.31(2.18)	1.77(1.09)	15.50(40.90)
0.8	0.5	3.18(0.04)	0.47(0.02)	6.84(0.31)	2.26(1.03)	1.86(1.32)	1.18(0.69)	4.68(4.26)
0.8	0.6	3.32(0.03)	0.48(0.02)	6.88(0.29)	2.11(1.10)	3.52(4.71)	1.30(0.92)	14.13(30.41)
0.8	0.7	3.28(0.03)	0.49(0.02)	6.73(0.22)	1.36(1.60)	6.64(6.66)	0.99(0.99)	9.77(11.11)
0.8	0.8	3.26(0.06)	0.47(0.03)	7.03(0.50)	1.92(1.44)	3.26(4.03)	1.68(1.25)	5.31(7.72)
0.8	0.9	3.47(0.03)	0.49(0.02)	7.08(0.27)	1.54(0.77)	3.35(2.41)	1.59(1.33)	18.50(40.33)
0.8	1.0	3.42(0.07)	0.49(0.02)	6.93(0.34)	2.06(1.19)	2.47(1.53)	1.85(1.10)	5.23(7.45)
1.0	0.1	2.23(0.02)	0.30(0.03)	7.73(0.72)	1.76(1.13)	3.86(6.72)	1.89(1.18)	2.53(3.85)
1.0	0.2	2.45(0.03)	0.31(0.04)	7.88(0.95)	2.33(1.79)	9.41(22.71)	0.83(0.52)	4.52(2.78)
1.0	0.3	2.66(0.04)	0.35(0.04)	7.87(0.74)	1.56(1.15)	8.15(14.80)	1.84(1.34)	2.11(1.37)
1.0	0.4	2.84(0.07)	0.37(0.03)	7.63(0.49)	1.97(1.63)	6.16(10.34)	1.10(0.81)	5.83(6.36)
1.0	0.5	2.84(0.04)	0.39(0.03)	7.34(0.61)	1.72(1.23)	3.63(4.71)	1.82(1.38)	7.43(14.99)
1.0	0.6	2.82(0.04)	0.41(0.04)	6.93(0.59)	2.30(1.18)	1.63(0.71)	1.98(1.21)	2.69(3.40)
1.0	0.7	2.93(0.03)	0.43(0.03)	6.92(0.39)	1.90(1.17)	4.21(5.75)	1.57(1.33)	10.83(18.10)
1.0	0.8	3.10(0.04)	0.43(0.04)	7.25(0.65)	1.88(0.93)	2.56(1.98)	1.72(1.00)	6.66(14.53)
1.0	0.9	3.28(0.02)	0.46(0.02)	7.23(0.31)	2.13(1.37)	3.60(4.59)	1.04(0.99)	5.39(3.76)
1.0	1.0	3.38(0.02)	0.46(0.02)	7.46(0.26)	1.71(0.99)	3.28(2.79)	1.86(1.18)	4.94(8.89)
1.2	0.1	1.99(0.02)	0.24(0.03)	8.63(0.92)	1.22(1.30)	5.52(4.64)	1.51(1.36)	9.00(17.51)
1.2	0.2	2.10(0.07)	0.27(0.02)	7.83(0.80)	0.70(0.48)	5.19(4.74)	1.37(0.94)	1.94(1.16)
1.2	0.3	2.32(0.05)	0.30(0.02)	7.91(0.71)	1.71(1.37)	2.77(3.32)	1.50(0.64)	4.67(9.31)
1.2	0.4	2.48(0.01)	0.32(0.03)	7.73(0.67)	1.34(0.69)	2.71(2.42)	1.70(1.18)	2.50(2.39)
1.2	0.5	2.66(0.06)	0.34(0.04)	7.97(0.70)	1.28(0.59)	2.32(1.08)	1.89(1.27)	9.55(21.16)
1.2	0.6	2.75(0.07)	0.35(0.02)	7.89(0.56)	1.62(1.22)	9.61(22.48)	1.14(0.60)	3.43(2.15)
1.2	0.7	2.79(0.02)	0.37(0.03)	7.58(0.61)	2.12(1.46)	9.80(24.50)	1.65(0.82)	2.40(2.24)
1.2	0.8	2.87(0.07)	0.38(0.03)	7.59(0.63)	1.60(1.31)	14.86(36.81)	1.67(1.44)	4.31(5.32)
1.2	0.9	3.07(0.04)	0.41(0.03)	7.66(0.63)	2.15(1.14)	7.33(17.54)	1.67(0.95)	3.36(3.06)
1.2	1.0	3.17(0.05)	0.43(0.02)	7.46(0.46)	1.52(1.52)	21.41(54.65)	1.14(0.76)	8.50(13.81)

TABLE VI. Mean and standard deviation (in parenthesis) for the contact layer density ρ_c , density depletion layer thickness δ_{LS} , maximum of the in-plane static structure factor of the contact layer S_{max} , contact layer temperature T_c , interface temperature drop ΔT and thermal slip length L_T measured at the hotter and colder L/S interface for $(T_{source}, T_{sink}) = (1.8, 0.8)$, $\sigma_{LS} = 0.8, 1.0$ and 1.2 and $\varepsilon_{LS} = 0.1, 0.2, \dots, 0.9, 1.0$. All quantities are in reduced units given in Table I. (Entries must be multiplied by the numerical factor in the column heading).

Hotter L/S interface							Colder L/S interface						
σ_{LS}	ε_{LS}	ρ_c	δ_{LS}	S_{max}	T_c	ΔT	L_T	ρ_c	δ_{LS}	S_{max}	T_c	ΔT	L_T
0.8	0.1	0.922(0.018)	0.646(0.008)	0.139(0.001)	1.618(0.007)	0.176(0.007)	8.871(0.386)	0.995(0.019)	0.465(0.010)	0.507(0.008)	0.973(0.005)	0.147(0.007)	7.377(0.398)
0.8	0.2	1.021(0.009)	0.657(0.009)	0.147(0.002)	1.627(0.006)	0.165(0.005)	8.097(0.317)	1.263(0.015)	0.487(0.007)	0.473(0.003)	0.970(0.002)	0.141(0.006)	6.908(0.378)
0.8	0.3	1.075(0.029)	0.665(0.008)	0.156(0.002)	1.629(0.008)	0.166(0.007)	7.926(0.419)	1.474(0.031)	0.468(0.000)	0.539(0.004)	0.955(0.005)	0.124(0.006)	5.933(0.355)
0.8	0.4	1.116(0.013)	0.666(0.008)	0.171(0.001)	1.634(0.007)	0.157(0.010)	7.313(0.556)	1.774(0.031)	0.452(0.000)	0.631(0.006)	0.943(0.003)	0.111(0.004)	5.142(0.225)
0.8	0.5	1.153(0.011)	0.655(0.000)	0.190(0.002)	1.641(0.006)	0.152(0.008)	6.901(0.419)	2.113(0.028)	0.452(0.000)	0.720(0.004)	0.931(0.003)	0.098(0.003)	4.469(0.159)
0.8	0.6	1.195(0.018)	0.643(0.007)	0.209(0.002)	1.657(0.004)	0.141(0.008)	6.194(0.393)	2.492(0.039)	0.437(0.000)	0.796(0.003)	0.920(0.004)	0.087(0.005)	3.816(0.238)
0.8	0.7	1.217(0.014)	0.638(0.005)	0.238(0.003)	1.664(0.004)	0.130(0.009)	5.628(0.418)	2.845(0.048)	0.437(0.000)	0.842(0.003)	0.915(0.002)	0.080(0.004)	3.467(0.176)
0.8	0.8	1.245(0.032)	0.629(0.008)	0.261(0.002)	1.673(0.004)	0.123(0.010)	5.193(0.494)	3.134(0.044)	0.435(0.005)	0.870(0.002)	0.907(0.003)	0.073(0.004)	3.073(0.155)
0.8	0.9	1.293(0.026)	0.622(0.005)	0.295(0.002)	1.680(0.006)	0.118(0.005)	4.920(0.222)	3.383(0.049)	0.431(0.008)	0.887(0.001)	0.901(0.003)	0.067(0.005)	2.773(0.216)
0.8	1.0	1.340(0.019)	0.608(0.000)	0.325(0.003)	1.691(0.004)	0.106(0.006)	4.310(0.269)	3.589(0.027)	0.431(0.008)	0.899(0.001)	0.895(0.003)	0.060(0.003)	2.420(0.153)
1.0	0.1	1.292(0.036)	0.847(0.008)	0.073(0.001)	1.562(0.004)	0.217(0.005)	14.052(0.425)	1.641(0.029)	0.811(0.000)	0.142(0.002)	1.088(0.004)	0.260(0.006)	16.845(0.382)
1.0	0.2	1.381(0.022)	0.883(0.008)	0.081(0.001)	1.570(0.009)	0.207(0.008)	12.722(0.765)	1.822(0.009)	0.842(0.000)	0.174(0.002)	1.068(0.003)	0.239(0.006)	14.655(0.643)
1.0	0.3	1.456(0.021)	0.891(0.005)	0.092(0.001)	1.582(0.007)	0.190(0.009)	10.903(0.616)	1.994(0.026)	0.842(0.000)	0.222(0.003)	1.053(0.005)	0.216(0.005)	12.359(0.406)
1.0	0.4	1.536(0.025)	0.891(0.005)	0.106(0.001)	1.590(0.009)	0.188(0.009)	10.339(0.561)	2.160(0.026)	0.838(0.008)	0.281(0.003)	1.031(0.004)	0.195(0.005)	10.743(0.356)
1.0	0.5	1.596(0.024)	0.892(0.007)	0.119(0.001)	1.603(0.006)	0.176(0.008)	9.226(0.525)	2.386(0.037)	0.827(0.000)	0.356(0.006)	1.015(0.005)	0.178(0.007)	9.308(0.459)
1.0	0.6	1.646(0.034)	0.903(0.005)	0.135(0.001)	1.614(0.004)	0.163(0.004)	8.145(0.243)	2.630(0.041)	0.827(0.000)	0.453(0.005)	0.998(0.004)	0.161(0.004)	8.053(0.257)
1.0	0.7	1.716(0.035)	0.900(0.008)	0.152(0.002)	1.625(0.008)	0.154(0.007)	7.484(0.428)	3.016(0.051)	0.811(0.000)	0.561(0.005)	0.984(0.003)	0.146(0.005)	7.061(0.323)
1.0	0.8	1.770(0.017)	0.889(0.000)	0.171(0.001)	1.635(0.006)	0.149(0.005)	7.037(0.306)	3.390(0.030)	0.811(0.000)	0.670(0.004)	0.972(0.003)	0.132(0.003)	6.220(0.157)
1.0	0.9	1.862(0.029)	0.889(0.000)	0.192(0.001)	1.637(0.008)	0.140(0.009)	6.443(0.452)	3.759(0.052)	0.805(0.008)	0.746(0.004)	0.963(0.005)	0.123(0.005)	5.641(0.185)
1.0	1.0	1.933(0.023)	0.889(0.000)	0.214(0.002)	1.651(0.007)	0.131(0.007)	5.836(0.356)	4.079(0.053)	0.797(0.005)	0.795(0.002)	0.951(0.002)	0.110(0.004)	4.894(0.225)
1.2	0.1	1.439(0.027)	1.045(0.000)	0.048(0.001)	1.527(0.011)	0.250(0.012)	19.648(1.642)	1.797(0.030)	1.022(0.008)	0.076(0.001)	1.145(0.004)	0.316(0.006)	24.821(1.281)
1.2	0.2	1.574(0.019)	1.078(0.005)	0.054(0.001)	1.537(0.006)	0.237(0.007)	17.257(0.792)	1.991(0.022)	1.062(0.005)	0.094(0.002)	1.126(0.005)	0.297(0.004)	21.613(0.574)
1.2	0.3	1.672(0.024)	1.100(0.008)	0.062(0.001)	1.549(0.007)	0.224(0.007)	14.973(0.574)	2.170(0.030)	1.076(0.000)	0.118(0.002)	1.102(0.004)	0.271(0.005)	18.148(0.413)
1.2	0.4	1.754(0.035)	1.108(0.000)	0.070(0.001)	1.565(0.007)	0.205(0.008)	12.768(0.625)	2.339(0.040)	1.086(0.008)	0.149(0.002)	1.087(0.003)	0.252(0.005)	15.680(0.409)
1.2	0.5	1.851(0.017)	1.123(0.000)	0.080(0.001)	1.573(0.008)	0.200(0.006)	11.857(0.512)	2.544(0.031)	1.092(0.000)	0.189(0.003)	1.065(0.003)	0.229(0.004)	13.582(0.350)
1.2	0.6	1.913(0.030)	1.123(0.000)	0.090(0.001)	1.585(0.005)	0.187(0.007)	10.485(0.459)	2.777(0.035)	1.092(0.000)	0.238(0.003)	1.050(0.004)	0.210(0.006)	11.726(0.404)
1.2	0.7	2.021(0.033)	1.125(0.005)	0.104(0.001)	1.592(0.004)	0.176(0.005)	9.431(0.365)	2.983(0.035)	1.090(0.005)	0.302(0.005)	1.035(0.005)	0.194(0.007)	10.426(0.510)
1.2	0.8	2.078(0.024)	1.126(0.007)	0.114(0.002)	1.610(0.007)	0.161(0.008)	8.291(0.506)	3.215(0.033)	1.086(0.008)	0.375(0.007)	1.025(0.004)	0.180(0.005)	9.249(0.388)
1.2	0.9	2.172(0.026)	1.123(0.000)	0.131(0.002)	1.613(0.007)	0.159(0.004)	7.904(0.248)	3.534(0.034)	1.076(0.000)	0.475(0.006)	1.008(0.004)	0.165(0.006)	8.210(0.367)
1.2	1.0	2.259(0.031)	1.123(0.000)	0.142(0.001)	1.624(0.007)	0.150(0.007)	7.269(0.438)	3.824(0.047)	1.076(0.000)	0.577(0.008)	0.999(0.004)	0.156(0.005)	7.547(0.365)

TABLE VII. Mean and standard deviation (in parenthesis) for the contact layer density ρ_c , density depletion layer thickness δ_{LS} , maximum of the in-plane static structure factor of the contact layer S_{max} , contact layer temperature T_c , interface temperature drop ΔT and thermal slip length L_T measured at the hotter and colder L/S interface for $(T_{source}, T_{sink}) = (1.6, 1.0)$, $\sigma_{LS} = 0.8, 1.0$ and 1.2 and $\varepsilon_{LS} = 0.1, 0.2, \dots, 0.9, 1.0$. All quantities are in reduced units given in Table I. (Entries must be multiplied by the numerical factor in the column heading).

Hotter L/S interface							Colder L/S interface						
σ_{LS}	ε_{LS}	ρ_c	δ_{LS}	S_{max}	T_c	ΔT	L_T	ρ_c	δ_{LS}	S_{max}	T_c	ΔT	L_T
0.8	0.1	0.946(0.029)	0.624(0.007)	0.166(0.002)	1.493(0.003)	0.100(0.007)	8.330(0.739)	0.993(0.020)	0.512(0.010)	0.400(0.007)	1.101(0.004)	0.090(0.004)	7.440(0.354)
0.8	0.2	1.066(0.025)	0.629(0.008)	0.178(0.002)	1.500(0.005)	0.093(0.004)	7.472(0.430)	1.198(0.030)	0.546(0.000)	0.365(0.002)	1.102(0.003)	0.086(0.003)	6.928(0.317)
0.8	0.3	1.129(0.017)	0.640(0.000)	0.195(0.002)	1.500(0.005)	0.092(0.009)	7.268(0.833)	1.300(0.024)	0.537(0.008)	0.409(0.002)	1.095(0.003)	0.077(0.004)	6.075(0.427)
0.8	0.4	1.168(0.018)	0.632(0.008)	0.216(0.002)	1.507(0.007)	0.082(0.006)	6.221(0.558)	1.444(0.029)	0.513(0.005)	0.474(0.004)	1.089(0.004)	0.070(0.005)	5.332(0.393)
0.8	0.5	1.224(0.015)	0.627(0.007)	0.247(0.003)	1.514(0.007)	0.076(0.006)	5.679(0.556)	1.615(0.022)	0.493(0.008)	0.555(0.003)	1.082(0.005)	0.065(0.006)	4.800(0.476)
0.8	0.6	1.258(0.014)	0.616(0.008)	0.276(0.002)	1.518(0.007)	0.074(0.004)	5.334(0.373)	1.844(0.027)	0.484(0.000)	0.629(0.005)	1.075(0.004)	0.056(0.005)	4.049(0.379)
0.8	0.7	1.312(0.017)	0.607(0.005)	0.308(0.002)	1.520(0.006)	0.072(0.008)	5.125(0.659)	2.083(0.025)	0.468(0.000)	0.699(0.003)	1.071(0.003)	0.052(0.004)	3.685(0.330)
0.8	0.8	1.349(0.016)	0.593(0.000)	0.345(0.004)	1.531(0.006)	0.063(0.006)	4.380(0.479)	2.339(0.031)	0.468(0.000)	0.759(0.003)	1.066(0.004)	0.048(0.005)	3.337(0.393)
0.8	0.9	1.415(0.032)	0.576(0.005)	0.386(0.004)	1.534(0.004)	0.058(0.006)	3.974(0.463)	2.581(0.037)	0.456(0.007)	0.803(0.002)	1.060(0.004)	0.043(0.006)	2.939(0.407)
0.8	1.0	1.479(0.018)	0.560(0.005)	0.425(0.002)	1.537(0.005)	0.058(0.006)	3.932(0.473)	2.792(0.042)	0.443(0.008)	0.832(0.001)	1.057(0.003)	0.038(0.005)	2.546(0.332)
1.0	0.1	1.350(0.027)	0.841(0.005)	0.082(0.002)	1.454(0.008)	0.131(0.010)	13.930(1.421)	1.552(0.025)	0.813(0.005)	0.120(0.001)	1.171(0.005)	0.149(0.007)	15.911(1.003)
1.0	0.2	1.462(0.021)	0.872(0.005)	0.093(0.001)	1.458(0.007)	0.128(0.008)	12.975(1.070)	1.710(0.033)	0.842(0.000)	0.147(0.002)	1.157(0.004)	0.137(0.006)	13.913(0.698)
1.0	0.3	1.550(0.022)	0.889(0.000)	0.107(0.001)	1.471(0.008)	0.118(0.008)	11.241(1.139)	1.872(0.020)	0.849(0.008)	0.180(0.003)	1.148(0.007)	0.126(0.007)	12.070(1.085)
1.0	0.4	1.623(0.020)	0.889(0.000)	0.124(0.001)	1.474(0.007)	0.107(0.007)	9.701(0.797)	1.995(0.023)	0.858(0.000)	0.220(0.002)	1.139(0.003)	0.118(0.005)	10.652(0.653)
1.0	0.5	1.716(0.020)	0.886(0.007)	0.143(0.002)	1.483(0.007)	0.100(0.007)	8.588(0.805)	2.139(0.037)	0.852(0.008)	0.273(0.003)	1.127(0.007)	0.105(0.008)	8.992(0.855)
1.0	0.6	1.794(0.015)	0.881(0.008)	0.165(0.003)	1.492(0.005)	0.093(0.008)	7.688(0.823)	2.303(0.050)	0.842(0.000)	0.329(0.006)	1.118(0.004)	0.095(0.006)	7.819(0.580)
1.0	0.7	1.869(0.035)	0.878(0.008)	0.189(0.003)	1.498(0.006)	0.087(0.008)	6.893(0.780)	2.505(0.023)	0.839(0.007)	0.402(0.003)	1.110(0.004)	0.085(0.006)	6.718(0.566)
1.0	0.8	1.954(0.027)	0.875(0.005)	0.215(0.002)	1.498(0.007)	0.085(0.005)	6.596(0.536)	2.721(0.037)	0.833(0.008)	0.479(0.004)	1.102(0.004)	0.078(0.005)	6.067(0.515)
1.0	0.9	2.025(0.030)	0.875(0.005)	0.242(0.002)	1.504(0.006)	0.080(0.008)	6.017(0.666)	2.989(0.033)	0.816(0.008)	0.562(0.005)	1.095(0.005)	0.071(0.007)	5.361(0.568)
1.0	1.0	2.112(0.025)	0.874(0.000)	0.270(0.002)	1.515(0.008)	0.075(0.005)	5.536(0.476)	3.279(0.031)	0.811(0.000)	0.640(0.007)	1.089(0.007)	0.069(0.008)	5.122(0.681)
1.2	0.1	1.514(0.017)	1.045(0.000)	0.051(0.001)	1.431(0.006)	0.156(0.007)	20.334(1.460)	1.701(0.020)	1.039(0.008)	0.069(0.001)	1.197(0.003)	0.183(0.003)	23.918(1.048)
1.2	0.2	1.637(0.029)	1.076(0.000)	0.059(0.001)	1.436(0.008)	0.148(0.008)	17.882(1.652)	1.897(0.035)	1.073(0.007)	0.084(0.001)	1.188(0.007)	0.170(0.006)	20.539(1.536)
1.2	0.3	1.752(0.034)	1.094(0.005)	0.069(0.001)	1.443(0.006)	0.141(0.009)	15.586(1.435)	2.077(0.021)	1.081(0.008)	0.103(0.002)	1.176(0.005)	0.154(0.003)	17.080(0.793)
1.2	0.4	1.856(0.024)	1.108(0.000)	0.080(0.001)	1.457(0.005)	0.125(0.004)	12.851(0.638)	2.208(0.016)	1.092(0.000)	0.126(0.002)	1.167(0.005)	0.147(0.006)	15.092(0.962)
1.2	0.5	1.968(0.024)	1.109(0.005)	0.093(0.001)	1.465(0.008)	0.120(0.006)	11.744(0.748)	2.390(0.045)	1.092(0.000)	0.157(0.003)	1.155(0.005)	0.135(0.002)	13.289(0.417)
1.2	0.6	2.031(0.027)	1.119(0.008)	0.105(0.001)	1.471(0.009)	0.111(0.009)	10.240(0.916)	2.541(0.026)	1.092(0.000)	0.188(0.003)	1.148(0.007)	0.123(0.008)	11.407(0.862)
1.2	0.7	2.149(0.039)	1.123(0.000)	0.121(0.002)	1.473(0.007)	0.109(0.004)	9.831(0.520)	2.717(0.040)	1.092(0.000)	0.227(0.003)	1.136(0.004)	0.117(0.006)	10.540(0.727)
1.2	0.8	2.251(0.019)	1.123(0.000)	0.139(0.001)	1.481(0.007)	0.100(0.007)	8.606(0.805)	2.863(0.032)	1.092(0.000)	0.273(0.003)	1.129(0.004)	0.105(0.006)	9.010(0.705)
1.2	0.9	2.346(0.022)	1.123(0.000)	0.158(0.001)	1.487(0.006)	0.091(0.006)	7.497(0.548)	3.046(0.020)	1.092(0.000)	0.329(0.004)	1.124(0.004)	0.100(0.006)	8.324(0.626)
1.2	1.0	2.439(0.035)	1.115(0.008)	0.177(0.002)	1.495(0.005)	0.086(0.005)	6.835(0.422)	3.300(0.054)	1.092(0.000)	0.394(0.004)	1.113(0.005)	0.090(0.005)	7.183(0.459)

TABLE VIII. Mean and standard deviation (in parenthesis) for the contact layer density ρ_c , density depletion layer thickness δ_{LS} , maximum of the in-plane static structure factor of the contact layer S_{max} , contact layer temperature T_c , interface temperature drop ΔT and thermal slip length L_T measured at the hotter and colder L/S interface for $(T_{source}, T_{sink}) = (1.4, 1.2)$, $\sigma_{LS} = 0.8, 1.0$ and 1.2 and $\varepsilon_{LS} = 0.1, 0.2, \dots, 0.9, 1.0$. All quantities are in reduced units given in Table I. (Entries must be multiplied by the numerical factor in the column heading).

Hotter L/S interface							Colder L/S interface						
σ_{LS}	ε_{LS}	ρ_c	δ_{LS}	S_{max}	T_c	ΔT	L_T	ρ_c	δ_{LS}	S_{max}	T_c	ΔT	L_T
0.8	0.1	0.973(0.019)	0.599(0.008)	0.213(0.003)	1.366(0.007)	0.028(0.004)	7.023(1.477)	0.949(0.018)	0.619(0.104)	0.324(0.009)	1.235(0.004)	0.033(0.007)	8.382(2.217)
0.8	0.2	1.106(0.019)	0.615(0.008)	0.223(0.002)	1.371(0.006)	0.028(0.005)	6.722(1.352)	1.145(0.017)	0.580(0.007)	0.280(0.003)	1.234(0.003)	0.031(0.004)	7.388(0.910)
0.8	0.3	1.186(0.017)	0.610(0.005)	0.252(0.002)	1.369(0.007)	0.027(0.008)	6.769(2.898)	1.247(0.016)	0.582(0.008)	0.318(0.002)	1.234(0.004)	0.032(0.003)	7.819(1.441)
0.8	0.4	1.248(0.016)	0.608(0.000)	0.278(0.002)	1.369(0.005)	0.025(0.006)	5.712(1.689)	1.317(0.023)	0.566(0.008)	0.362(0.003)	1.231(0.004)	0.025(0.004)	5.657(1.132)
0.8	0.5	1.282(0.023)	0.599(0.008)	0.315(0.002)	1.374(0.004)	0.019(0.005)	4.189(1.259)	1.390(0.023)	0.544(0.005)	0.414(0.004)	1.228(0.005)	0.023(0.005)	4.939(1.131)
0.8	0.6	1.353(0.029)	0.580(0.007)	0.354(0.002)	1.376(0.003)	0.016(0.008)	3.433(1.727)	1.526(0.024)	0.521(0.008)	0.477(0.004)	1.226(0.003)	0.021(0.007)	4.283(1.590)
0.8	0.7	1.418(0.014)	0.563(0.009)	0.404(0.003)	1.379(0.005)	0.017(0.004)	3.413(0.953)	1.660(0.021)	0.499(0.000)	0.539(0.004)	1.224(0.006)	0.019(0.005)	4.009(1.124)
0.8	0.8	1.511(0.026)	0.540(0.008)	0.454(0.004)	1.378(0.003)	0.019(0.006)	4.186(1.465)	1.822(0.030)	0.495(0.008)	0.603(0.002)	1.227(0.005)	0.022(0.006)	4.781(1.573)
0.8	0.9	1.614(0.024)	0.516(0.005)	0.508(0.004)	1.380(0.006)	0.014(0.005)	2.900(1.025)	2.018(0.055)	0.484(0.000)	0.661(0.004)	1.224(0.005)	0.018(0.005)	3.695(1.087)
0.8	1.0	1.771(0.015)	0.505(0.008)	0.567(0.003)	1.382(0.005)	0.013(0.007)	2.745(1.429)	2.196(0.033)	0.480(0.007)	0.715(0.002)	1.225(0.005)	0.018(0.008)	3.780(1.657)
1.0	0.1	1.414(0.033)	0.839(0.007)	0.094(0.001)	1.352(0.004)	0.045(0.006)	15.579(3.516)	1.472(0.016)	0.822(0.008)	0.105(0.002)	1.260(0.004)	0.054(0.004)	18.331(2.761)
1.0	0.2	1.531(0.036)	0.864(0.008)	0.107(0.002)	1.352(0.011)	0.041(0.010)	13.439(4.419)	1.628(0.026)	0.847(0.008)	0.125(0.002)	1.253(0.004)	0.051(0.006)	16.480(3.067)
1.0	0.3	1.638(0.029)	0.874(0.000)	0.126(0.001)	1.358(0.006)	0.036(0.008)	10.760(3.410)	1.742(0.025)	0.858(0.000)	0.148(0.002)	1.251(0.005)	0.046(0.008)	13.431(3.536)
1.0	0.4	1.736(0.029)	0.875(0.005)	0.149(0.002)	1.357(0.006)	0.033(0.006)	8.869(2.284)	1.874(0.031)	0.858(0.000)	0.178(0.002)	1.246(0.004)	0.040(0.004)	10.904(1.702)
1.0	0.5	1.839(0.030)	0.880(0.008)	0.175(0.002)	1.360(0.005)	0.032(0.008)	8.467(2.537)	1.966(0.039)	0.858(0.000)	0.214(0.002)	1.242(0.007)	0.036(0.007)	9.263(2.347)
1.0	0.6	1.925(0.039)	0.877(0.007)	0.203(0.002)	1.364(0.007)	0.028(0.008)	6.953(2.313)	2.111(0.016)	0.858(0.000)	0.255(0.003)	1.242(0.005)	0.033(0.006)	8.112(1.942)
1.0	0.7	2.027(0.033)	0.867(0.008)	0.234(0.002)	1.369(0.005)	0.025(0.004)	5.818(1.220)	2.215(0.041)	0.858(0.000)	0.302(0.004)	1.239(0.004)	0.032(0.006)	7.474(1.686)
1.0	0.8	2.132(0.020)	0.863(0.008)	0.272(0.003)	1.370(0.004)	0.024(0.007)	5.695(2.158)	2.341(0.028)	0.852(0.008)	0.352(0.003)	1.233(0.006)	0.030(0.008)	7.095(2.375)
1.0	0.9	2.238(0.021)	0.858(0.000)	0.310(0.002)	1.373(0.004)	0.023(0.005)	5.094(1.096)	2.529(0.040)	0.842(0.000)	0.412(0.004)	1.229(0.003)	0.025(0.005)	5.542(1.161)
1.0	1.0	2.344(0.021)	0.855(0.007)	0.354(0.003)	1.373(0.006)	0.021(0.005)	4.574(1.118)	2.687(0.025)	0.841(0.005)	0.471(0.003)	1.230(0.005)	0.025(0.006)	5.394(1.397)
1.2	0.1	1.575(0.027)	1.041(0.008)	0.057(0.001)	1.342(0.006)	0.054(0.009)	23.224(6.058)	1.637(0.026)	1.044(0.005)	0.062(0.001)	1.268(0.005)	0.065(0.006)	28.098(4.700)
1.2	0.2	1.710(0.025)	1.076(0.000)	0.065(0.001)	1.343(0.005)	0.053(0.005)	19.911(3.191)	1.800(0.019)	1.076(0.000)	0.073(0.001)	1.261(0.008)	0.056(0.005)	21.058(3.257)
1.2	0.3	1.845(0.023)	1.092(0.000)	0.078(0.001)	1.347(0.006)	0.048(0.007)	16.513(3.461)	1.958(0.023)	1.090(0.005)	0.090(0.001)	1.258(0.004)	0.050(0.005)	17.104(2.421)
1.2	0.4	1.947(0.019)	1.100(0.008)	0.092(0.002)	1.351(0.006)	0.042(0.005)	13.374(2.473)	2.087(0.022)	1.108(0.000)	0.107(0.001)	1.256(0.006)	0.047(0.005)	14.870(2.902)
1.2	0.5	2.079(0.035)	1.108(0.000)	0.108(0.002)	1.355(0.009)	0.041(0.009)	12.002(3.082)	2.224(0.028)	1.103(0.008)	0.128(0.002)	1.251(0.006)	0.043(0.009)	12.753(3.622)
1.2	0.6	2.223(0.031)	1.108(0.000)	0.127(0.002)	1.354(0.006)	0.035(0.007)	10.064(2.430)	2.346(0.042)	1.101(0.008)	0.152(0.002)	1.252(0.004)	0.045(0.005)	12.803(1.907)
1.2	0.7	2.312(0.041)	1.109(0.005)	0.147(0.003)	1.360(0.005)	0.033(0.007)	8.908(2.334)	2.514(0.037)	1.098(0.008)	0.183(0.002)	1.247(0.004)	0.040(0.007)	10.875(2.502)
1.2	0.8	2.434(0.027)	1.108(0.000)	0.168(0.002)	1.363(0.006)	0.032(0.006)	8.517(2.008)	2.651(0.045)	1.097(0.008)	0.212(0.003)	1.244(0.005)	0.038(0.008)	10.158(2.714)
1.2	0.9	2.556(0.036)	1.114(0.008)	0.195(0.002)	1.365(0.005)	0.027(0.005)	6.823(1.653)	2.762(0.025)	1.097(0.008)	0.249(0.002)	1.240(0.004)	0.034(0.007)	8.481(2.092)
1.2	1.0	2.669(0.042)	1.111(0.007)	0.222(0.002)	1.365(0.006)	0.027(0.008)	6.427(2.324)	2.924(0.047)	1.094(0.005)	0.286(0.002)	1.237(0.004)	0.031(0.002)	7.228(0.766)

TABLE IX. Mean and standard deviation (in parenthesis) for peak vibrational frequencies ν_L and ν_S and ratio ν_S/ν_L extracted from Eq. (A.13) for particles in the contact (L) layer and first solid (S) layer at the hotter and colder L/S interface for $(T_{\text{source}}, T_{\text{sink}}) = (1.8, 0.8)$, $\sigma_{LS} = 0.8, 1.0$ and 1.2 and $\varepsilon_{LS} = 0.1, 0.2, \dots, 0.8, 1.0$. All quantities are in reduced units given in Table I.

σ_{LS}	ε_{LS}	Hotter L/S interface			Colder L/S interface		
		ν_L	ν_S	ν_S/ν_L	ν_L	ν_S	ν_S/ν_L
0.8	0.1	2.453(0.021)	4.843(0.006)	1.974(0.015)	2.377(0.006)	5.070(0.000)	2.133(0.005)
0.8	0.2	1.050(0.000)	4.870(0.014)	4.638(0.013)	1.563(0.055)	5.120(0.000)	3.278(0.115)
0.8	0.3	1.123(0.012)	4.900(0.000)	4.362(0.045)	1.660(0.062)	5.147(0.006)	3.103(0.118)
0.8	0.4	1.150(0.017)	4.913(0.006)	4.273(0.066)	1.740(0.017)	5.183(0.006)	2.979(0.026)
0.8	0.5	1.200(0.010)	4.920(0.000)	4.100(0.034)	1.857(0.015)	5.227(0.012)	2.815(0.023)
0.8	0.6	1.243(0.021)	4.937(0.006)	3.971(0.068)	1.947(0.012)	5.260(0.000)	2.702(0.016)
0.8	0.7	1.337(0.021)	4.950(0.010)	3.704(0.060)	2.037(0.012)	5.300(0.000)	2.602(0.015)
0.8	0.8	1.390(0.026)	4.967(0.006)	3.574(0.066)	2.150(0.010)	5.343(0.012)	2.485(0.013)
0.8	0.9	1.443(0.055)	4.987(0.006)	3.458(0.137)	2.230(0.010)	5.387(0.006)	2.416(0.013)
0.8	1.0	1.503(0.031)	5.007(0.012)	3.331(0.076)	2.330(0.010)	5.427(0.006)	2.329(0.008)
1.0	0.1	1.073(0.006)	4.923(0.006)	4.587(0.019)	1.317(0.032)	5.150(0.000)	3.913(0.097)
1.0	0.2	1.133(0.029)	4.950(0.000)	4.370(0.113)	1.437(0.006)	5.173(0.006)	3.601(0.013)
1.0	0.3	1.177(0.031)	4.963(0.006)	4.220(0.104)	1.527(0.060)	5.203(0.006)	3.412(0.137)
1.0	0.4	1.230(0.020)	4.983(0.006)	4.052(0.066)	1.583(0.025)	5.243(0.006)	3.312(0.049)
1.0	0.5	1.300(0.030)	5.007(0.006)	3.853(0.093)	1.700(0.040)	5.283(0.006)	3.109(0.070)
1.0	0.6	1.360(0.090)	5.030(0.010)	3.709(0.239)	1.877(0.064)	5.327(0.012)	2.840(0.088)
1.0	0.7	1.350(0.026)	5.050(0.010)	3.742(0.067)	1.990(0.061)	5.377(0.006)	2.704(0.085)
1.0	0.8	1.403(0.032)	5.083(0.006)	3.624(0.078)	2.160(0.020)	5.430(0.017)	2.514(0.017)
1.0	0.9	1.450(0.026)	5.100(0.017)	3.518(0.053)	2.313(0.023)	5.503(0.006)	2.379(0.025)
1.0	1.0	1.527(0.038)	5.147(0.025)	3.372(0.072)	2.433(0.006)	5.560(0.000)	2.285(0.005)
1.2	0.1	1.120(0.017)	4.960(0.000)	4.429(0.068)	1.347(0.025)	5.170(0.000)	3.840(0.072)
1.2	0.2	1.183(0.021)	4.980(0.000)	4.209(0.075)	1.410(0.017)	5.197(0.012)	3.686(0.042)
1.2	0.3	1.240(0.035)	5.010(0.010)	4.043(0.122)	1.487(0.031)	5.237(0.012)	3.523(0.074)
1.2	0.4	1.330(0.040)	5.047(0.006)	3.797(0.114)	1.633(0.021)	5.267(0.015)	3.225(0.032)
1.2	0.5	1.393(0.032)	5.070(0.010)	3.640(0.082)	1.670(0.010)	5.323(0.012)	3.188(0.014)
1.2	0.6	1.397(0.076)	5.110(0.010)	3.666(0.211)	1.800(0.017)	5.360(0.000)	2.978(0.029)
1.2	0.7	1.500(0.046)	5.143(0.012)	3.431(0.098)	1.897(0.006)	5.427(0.006)	2.861(0.006)
1.2	0.8	1.523(0.045)	5.183(0.012)	3.405(0.107)	2.053(0.025)	5.480(0.010)	2.669(0.031)
1.2	0.9	1.573(0.012)	5.227(0.006)	3.322(0.021)	2.213(0.021)	5.523(0.006)	2.496(0.026)
1.2	1.0	1.627(0.035)	5.283(0.012)	3.249(0.076)	2.363(0.012)	5.567(0.012)	2.355(0.016)

TABLE X. Mean and standard deviation (in parenthesis) for peak vibrational frequencies ν_L and ν_S and ratio ν_S/ν_L extracted from Eq. (A.13) for particles in the contact (L) layer and first solid (S) layer at the hotter and colder L/S interface for $(T_{\text{source}}, T_{\text{sink}}) = (1.6, 1.0)$, $\sigma_{LS} = 0.8, 1.0$ and 1.2 and $\varepsilon_{LS} = 0.1, 0.2, \dots, 0.8, 1.0$. All quantities are in reduced units given in Table I.

σ_{LS}	ε_{LS}	Hotter L/S interface			Colder L/S interface		
		ν_L	ν_S	ν_S/ν_L	ν_L	ν_S	ν_S/ν_L
0.8	0.1	2.407(0.012)	4.903(0.006)	2.037(0.007)	2.383(0.006)	5.047(0.006)	2.117(0.004)
0.8	0.2	1.170(0.036)	4.947(0.006)	4.230(0.125)	1.483(0.038)	5.080(0.000)	3.426(0.089)
0.8	0.3	1.207(0.006)	4.963(0.006)	4.113(0.018)	1.547(0.025)	5.110(0.010)	3.304(0.057)
0.8	0.4	1.280(0.036)	4.980(0.000)	3.893(0.111)	1.617(0.038)	5.137(0.006)	3.178(0.072)
0.8	0.5	1.330(0.035)	4.997(0.006)	3.759(0.102)	1.697(0.038)	5.170(0.000)	3.048(0.067)
0.8	0.6	1.403(0.029)	5.010(0.000)	3.571(0.074)	1.733(0.031)	5.200(0.000)	3.001(0.053)
0.8	0.7	1.453(0.067)	5.023(0.012)	3.461(0.162)	1.833(0.021)	5.237(0.006)	2.857(0.030)
0.8	0.8	1.490(0.010)	5.047(0.006)	3.387(0.019)	1.957(0.023)	5.283(0.006)	2.700(0.031)
0.8	0.9	1.563(0.049)	5.067(0.015)	3.243(0.100)	2.070(0.017)	5.320(0.000)	2.570(0.022)
0.8	1.0	1.643(0.070)	5.090(0.000)	3.101(0.133)	2.120(0.010)	5.353(0.006)	2.525(0.012)
1.0	0.1	1.137(0.051)	4.970(0.010)	4.379(0.208)	1.307(0.032)	5.113(0.006)	3.915(0.096)
1.0	0.2	1.193(0.025)	5.003(0.006)	4.194(0.089)	1.407(0.023)	5.147(0.006)	3.659(0.057)
1.0	0.3	1.230(0.026)	5.020(0.010)	4.083(0.097)	1.467(0.087)	5.167(0.006)	3.531(0.211)
1.0	0.4	1.310(0.020)	5.047(0.006)	3.853(0.055)	1.500(0.053)	5.200(0.000)	3.469(0.120)
1.0	0.5	1.370(0.000)	5.073(0.006)	3.703(0.004)	1.570(0.040)	5.243(0.006)	3.341(0.085)
1.0	0.6	1.377(0.021)	5.103(0.006)	3.708(0.059)	1.633(0.042)	5.277(0.012)	3.232(0.087)
1.0	0.7	1.463(0.101)	5.127(0.012)	3.514(0.238)	1.803(0.067)	5.323(0.006)	2.955(0.108)
1.0	0.8	1.523(0.025)	5.157(0.006)	3.386(0.053)	1.890(0.053)	5.383(0.006)	2.850(0.081)
1.0	0.9	1.607(0.049)	5.197(0.015)	3.236(0.092)	2.020(0.030)	5.437(0.006)	2.692(0.040)
1.0	1.0	1.633(0.032)	5.237(0.006)	3.207(0.061)	2.173(0.040)	5.510(0.000)	2.536(0.047)
1.2	0.1	1.160(0.062)	5.007(0.015)	4.324(0.216)	1.287(0.032)	5.130(0.000)	3.989(0.101)
1.2	0.2	1.247(0.021)	5.037(0.006)	4.041(0.064)	1.350(0.085)	5.170(0.000)	3.840(0.241)
1.2	0.3	1.303(0.047)	5.067(0.006)	3.891(0.145)	1.463(0.032)	5.200(0.000)	3.555(0.077)
1.2	0.4	1.340(0.036)	5.100(0.000)	3.808(0.104)	1.523(0.032)	5.250(0.010)	3.447(0.071)
1.2	0.5	1.440(0.017)	5.130(0.000)	3.563(0.043)	1.577(0.015)	5.287(0.015)	3.353(0.023)
1.2	0.6	1.477(0.006)	5.173(0.006)	3.503(0.012)	1.697(0.040)	5.333(0.015)	3.145(0.080)
1.2	0.7	1.530(0.026)	5.213(0.015)	3.408(0.059)	1.760(0.036)	5.387(0.006)	3.061(0.065)
1.2	0.8	1.587(0.065)	5.267(0.012)	3.323(0.131)	1.883(0.012)	5.443(0.012)	2.890(0.022)
1.2	0.9	1.647(0.071)	5.317(0.006)	3.233(0.138)	1.980(0.035)	5.493(0.015)	2.775(0.048)
1.2	1.0	1.683(0.029)	5.350(0.010)	3.179(0.055)	2.090(0.035)	5.543(0.015)	2.653(0.046)

TABLE XI. Mean and standard deviation (in parenthesis) for peak vibrational frequencies ν_L and ν_S and ratio ν_S/ν_L extracted from Eq. (A.13) for particles in the contact (L) layer and first solid (S) layer at the hotter and colder L/S interface for $(T_{\text{source}}, T_{\text{sink}}) = (1.4, 1.2)$, $\sigma_{LS} = 0.8, 1.0$ and 1.2 and $\varepsilon_{LS} = 0.1, 0.2, \dots, 0.8, 1.0$. All quantities are in reduced units given in Table I.

σ_{LS}	ε_{LS}	Hotter L/S interface			Colder L/S interface		
		ν_L	ν_S	ν_S/ν_L	ν_L	ν_S	ν_S/ν_L
0.8	0.1	2.397(0.015)	4.960(0.000)	2.070(0.013)	2.390(0.017)	5.010(0.000)	2.096(0.015)
0.8	0.2	1.243(0.006)	4.990(0.000)	4.013(0.019)	1.323(0.023)	5.040(0.000)	3.809(0.066)
0.8	0.3	1.323(0.029)	5.017(0.006)	3.792(0.086)	1.440(0.026)	5.067(0.006)	3.519(0.062)
0.8	0.4	1.390(0.036)	5.037(0.006)	3.625(0.097)	1.450(0.078)	5.093(0.006)	3.519(0.186)
0.8	0.5	1.457(0.038)	5.053(0.006)	3.471(0.085)	1.557(0.032)	5.117(0.006)	3.288(0.065)
0.8	0.6	1.543(0.006)	5.073(0.006)	3.287(0.009)	1.657(0.050)	5.137(0.006)	3.102(0.091)
0.8	0.7	1.577(0.031)	5.100(0.010)	3.236(0.069)	1.663(0.042)	5.167(0.006)	3.108(0.080)
0.8	0.8	1.637(0.040)	5.127(0.006)	3.134(0.077)	1.790(0.035)	5.203(0.006)	2.908(0.052)
0.8	0.9	1.690(0.040)	5.150(0.010)	3.049(0.075)	1.860(0.017)	5.233(0.015)	2.814(0.029)
0.8	1.0	1.753(0.050)	5.177(0.006)	2.954(0.086)	1.940(0.053)	5.273(0.006)	2.719(0.070)
1.0	0.1	1.167(0.032)	5.023(0.012)	4.308(0.127)	1.220(0.062)	5.067(0.006)	4.160(0.205)
1.0	0.2	1.210(0.044)	5.057(0.006)	4.183(0.149)	1.307(0.035)	5.097(0.006)	3.902(0.106)
1.0	0.3	1.287(0.015)	5.073(0.006)	3.943(0.044)	1.367(0.015)	5.123(0.006)	3.749(0.039)
1.0	0.4	1.333(0.046)	5.107(0.006)	3.833(0.138)	1.437(0.006)	5.157(0.006)	3.589(0.010)
1.0	0.5	1.473(0.045)	5.130(0.000)	3.484(0.106)	1.463(0.047)	5.190(0.000)	3.549(0.116)
1.0	0.6	1.500(0.030)	5.160(0.000)	3.441(0.069)	1.573(0.100)	5.227(0.006)	3.331(0.220)
1.0	0.7	1.590(0.036)	5.193(0.006)	3.267(0.072)	1.663(0.029)	5.273(0.012)	3.171(0.059)
1.0	0.8	1.640(0.104)	5.237(0.006)	3.201(0.194)	1.787(0.045)	5.317(0.006)	2.977(0.076)
1.0	0.9	1.657(0.061)	5.283(0.006)	3.192(0.123)	1.860(0.017)	5.363(0.006)	2.884(0.028)
1.0	1.0	1.733(0.023)	5.343(0.012)	3.083(0.038)	1.880(0.036)	5.420(0.017)	2.884(0.064)
1.2	0.1	1.193(0.040)	5.057(0.006)	4.241(0.140)	1.240(0.036)	5.100(0.000)	4.115(0.118)
1.2	0.2	1.250(0.072)	5.087(0.006)	4.078(0.235)	1.323(0.021)	5.120(0.000)	3.870(0.061)
1.2	0.3	1.357(0.015)	5.127(0.012)	3.779(0.051)	1.370(0.046)	5.167(0.012)	3.774(0.127)
1.2	0.4	1.443(0.067)	5.153(0.006)	3.576(0.165)	1.467(0.021)	5.197(0.006)	3.544(0.054)
1.2	0.5	1.493(0.021)	5.193(0.015)	3.478(0.059)	1.560(0.066)	5.243(0.006)	3.365(0.143)
1.2	0.6	1.553(0.032)	5.237(0.006)	3.372(0.067)	1.593(0.021)	5.287(0.012)	3.318(0.039)
1.2	0.7	1.600(0.082)	5.280(0.000)	3.306(0.172)	1.700(0.020)	5.340(0.010)	3.141(0.034)
1.2	0.8	1.690(0.036)	5.333(0.006)	3.157(0.064)	1.787(0.021)	5.400(0.010)	3.023(0.034)
1.2	0.9	1.750(0.046)	5.380(0.000)	3.076(0.081)	1.843(0.070)	5.440(0.000)	2.954(0.113)
1.2	1.0	1.793(0.032)	5.430(0.010)	3.029(0.059)	1.917(0.029)	5.493(0.012)	2.867(0.049)